Received: 12 January 2025 | Accepted: 1 October 2025

DOI: 10.1002/tpg2.70146

The Plant Genome

ORIGINAL ARTICLE

Special Section: From Seed to Pasta IV Congress

Genetic dissection of the root system architecture QTLome and its relationship with early shoot development, breeding and adaptation in durum wheat

Giuseppe Sciara[1] | **Matteo Bozzoli**[1] | **Fabio Fiorani**[2] | **Kerstin A. Nagel**[2] | **Amina Ameer**[1] | **Silvio Salvi**[1] | **Roberto Tuberosa**[1] | **Marco Maccaferri**[1]

[1]Department of Agricultural and Food Sciences (DISTAL), Alma Mater Studiorum–Università di Bologna, Bologna, Italy

[2]Institute of Biosciences and Geosciences (IBG-2): Plant Sciences, Forschungszentrum Julich GmbH, Juelich, Germany

Correspondence
Marco Maccaferri, Department of Agricultural and Food Sciences (DISTAL), Alma Mater Studiorum–Università di Bologna, Bologna, 40127, Italy.
Email: marco.maccaferri@unibo.it

Assigned to Associate Editor Curtis Pozniak.

Funding information
FP7 European project, specific programme "cooperation": Food, Agriculture and Biotechnology, DROPS, "Drought-tolerant yielding plants", Grant/Award Number: ID : 244374; IWYP, International Wheat Yield Partnership, Rooty, "Rooty: A Root Ideotype Toolbox to Support Improved Wheat Yields"; IBG-2 Plant Science Institute, Forschungszentrum Jülich; AGER Agri-Food & Research project—Multidisciplinary approaches for a more sustainable and high-quality durum wheat production

Abstract

Root system architecture (RSA), shoot architecture, and shoot-to-root biomass allocation are critical for optimizing crop water and nutrient capture and ultimately grain yield. Nevertheless, only a few studies adequately dissected the genetic basis of RSA and its relationship to shoot development. Herein, we dissected at a high level of details the RSA–shoot QTLome in a panel of 194 elite durum wheat (*Triticum turgidum* ssp. *durum* Desf.) varieties from worldwide adopting high-throughput phenotyping platform (HTPP) and genome-wide association study (GWAS). Plants were grown in controlled conditions up to the seventh leaf appearance (late tillering) in the GROWSCREEN-Rhizo, a rhizobox platform integrated with automated monochrome camera for root imaging, which allowed us to phenotype the panel for 35 shoot and root architectural traits, including seminal, nodal, and lateral root traits, width and depth, leaf area, leaf, and tiller number on a time-course base. GWAS identified 180 quantitative trait loci (QTLs) ($-\log p$-value ≥ 4) grouped in 39 QTL clusters. Among those, 10, 11, and 10 QTL clusters were found for seminal, nodal, and lateral root systems. Deep rooting, a key trait for adaptation to water limiting conditions, was controlled by three major QTLs on chromosomes 2A, 6A, and 7A. Haplotype distribution revealed contrasting selection patterns between the ICARDA rainfed and CIMMYT irrigated breeding programs, respectively. These results provide valuable insights toward a better understanding of the RSA QTLome and a more

Abbreviations: BLUEs, best linear unbiased estimates; BW, bread wheat; CI, confidence interval; CIMMYT, International Maize and Wheat Improvement Center; DW, durum wheat; GWAS, genome-wide association study; ICARDA, International Center for Agricultural Research in the Dry Areas; LD, linkage disequilibrium; QTL, quantitative trait locus; RD75, root depth, 75th percentile (cm), whole root system; RSA, root system architecture; RSDW, root and shoot dry weight (g); RSL, root seminal length (cm), whole root system; RTL, root total length (cm), total root system; RW, root system width (cm), total root system; SDW, shoot dry weight (g); SLA, shoot, total leaf area (cm^2/leaf); SNP, single nucleotide polymorphism; SPAD, chlorophyll content; SSR, simple sequence repeat.

effective deployment of beneficial root haplotypes to enhance durum wheat yield in different environmental conditions.

Plain Language Summary

Root system architecture (RSA) and shoot-to-root partitioning are key for efficient crop use of water and nutrients. Optimizing RSA is a main breeding objective. Knowledge of the RSA QTLome is limited and RSA dissection in adult plants remains challenging. Therefore, it requires high-throughput phenotyping platforms (HTPPs). The GROWSCREEN-rhizo HTPP was used to phenotype a worldwide panel of 189 elite durum wheat varieties for up to 35 shoot and root traits. A GWAS detected 39 quantitative trait locus (QTL) clusters for multiple traits, including 10, 11, and 10 QTL clusters for seminal, nodal, and lateral root traits, mapped on the Svevo v1.0 reference genome. Three QTL clusters were prioritized. Single nucleotide polymorphism-based haplotypes were defined for the prioritized QTL clusters. Haplotype distribution revealed contrasting selection patterns between the ICARDA-rainfed and the CIMMYT-irrigated breeding programs. These results contribute to a better understanding of the RSA QTLome and deployment of beneficial haplotypes.

1 | INTRODUCTION

Durum wheat (DW) (*Triticum turgidum* subsp. *durum* Desf.) is the main carbohydrate source for the Mediterranean diet, one of the UNESCO-protected Intangible Cultural Heritages of Humanity. Durum represents around 7% only of the global wheat production (International Grain Council data, https://www.igc.int). However, DW ranks 10th worldwide among crops with an annual production of over 40 million t (Sall et al., 2019) and is a main cereal for semi-arid, rainfed-agricultural system areas, like the Mediterranean Basin, including Southern Europe, North African countries, Western and Central Asia like Turkey and Kazakhstan, Canada, North Dakota, Mexico, and India. Durum is an allotetraploid wheat ($2n = 4x = 28$, BBAA) that shares two-thirds of its genome with the hexaploid common or bread wheat (BW) (*Triticum aestivum*, $2n = 6x = 42$, BBAADD). Besides its economic value, durum and other tetraploid wheat represent a simplified polyploid model for wheat genetic studies and a large source of diversity for trait introgression in BW (Maccaferri et al., 2019; Mazzucotelli et al., 2020).

Global warming and drought waves are increasingly challenging agricultural crop productions, particularly in the semi-arid areas (Choudhari et al., 2019). Additionally, agricultural systems are called to increase their overall environmental and economic sustainability (Basso & Antle, 2020; Cooper & Messina, 2021; Liang et al., 2024). Therefore, main targets for contemporary breeding are improving resilience to abiotic stresses and efficiency of nutrient and water use (Hawkesford, 2017; Rebetzke et al., 2019; Varshney et al., 2020). In this frame, studies on root architecture and anatomy are crucial to understand the physiology and genetics of crops' adaptation to drought and limited nutrient availability, including their plasticity of growth response (Manschadi et al., 2006, 2008; Tuberosa & Salvi, 2006; Collins et al., 2008; Fleury et al., 2010; Lynch, 2013; Palta et al., 2011; Tuberosa, 2012; Wasson et al., 2012; Rich et al., 2016; Ober et al., 2021; Le Roux et al., 2024; Maqbool et al., 2022; Reynolds et al., 2021; Vadez et al., 2024; Wehis et al., 2024; Zeng et al., 2023).

As for drought, when crop development relies on the water stored in deep soil layers, as in rainfed Mediterranean and Mediterranean-like climates, the capability of the roots to access the deep soil layers and therefore the residual, stored water improves water uptake and efficiency of water use (Olivares-Villegas et al., 2007). This can be reached mainly based on enhanced root gravitropism, narrow root growth angle (RGA), and/or maintenance of root elongation (Ober et al., 2021; Fusi et al., 2022). Concerning narrow RGA, the most successful and notable example is the identification and exploitation of *DRO1* allele for steeper and deeper root system architecture (RSA) in rice (Uga et al., 2013), therefore increasing the ability to better cope with limited availability of water (Kitomi et al., 2020). Conversely, shallow root systems and greater root density in topsoil could be beneficial when the crop relies on drip irrigation or grows in shallow soils (El Hassouni et al., 2018; Ober et al., 2021; Nehe et al., 2021;

Odone et al., 2025; H. Li et al., 2025). As of today, several studies have shown how wheat varieties selected for growing in drought-prone environments are characterized by deeper roots, densely branched in the deepest soil layers (El Hassouni et al., 2018; Manschadi et al., 2006; Rich et al., 2016). RSA is also critical for efficient nutrient foraging in variable agronomic soil conditions (reviewed in Lynch, 2013; Koevoets et al., 2016). It is also well known that root-to-shoot ratio increases in response to low nutrient availability (de Souza Campos et al., 2019; Gioia et al., 2015).

Temperate small grain cereals like wheat are characterized by typical fibrous root systems (Diggle, 1988) defined by seminal, nodal/adventitious, and lateral roots with different ontogenesis, growing time, and variable number of axes and initiation times, growth rates, and branching (Manske & Vlek et al., 2002). Modeling and phenotyping are both challenging when dealing with fibrous root systems. The three root types of the wheat RSA have different ontogenesis and a partially different genetic control as well as different adaptive relevance (Diggle, 1988; Ito et al., 2006; Atkinson et al., 2015; Chen et al., 2019; Del Bianco & Kepinski, 2018; J. Guo et al., 2018; Kadam et al., 2015; Kenobi et al., 2017; York et al., 2018; Yu et al., 2016; Nouraei et al., 2024). Seminal roots develop earlier and can reach very deep soil layers (Howell et al., 2018); thus, seminal roots can be considered relevant for the plastic response to soil water deficits (Trejo et al., 2018). Nodal adventitious roots develop under post-embryonic development and contribute to most of the root biomass in the upper soil layers and nutrient and water foraging. Nodal root emission and development have been shown to respond to flood, heavy metal, water, and nutrient availability (Steffens & Rasmussen, 2016). Lateral roots show a wide variation and high plasticity in both number and length, and capacity to grow and elongate, particularly in response to water and nitrogen (Atkinson et al., 2015; Peng et al., 2019; Olatunji et al., 2017; Passot et al., 2018).

Direct phenotyping of thin and fibrous roots, such as those of small grain cereals and especially at the adult plant stage, poses serious practical problems and represents a bottleneck for genetics studies and drought-tolerance breeding (Nehe et al., 2021). It has been demonstrated that selecting cooler canopy temperature and senescence dynamics in the field is a promising and robust approach for indirectly screening for deeper root systems (Reynolds et al., 2009; Odone & Thorup-Kristensen, 2025). Direct adult plant-based investigation and RSA phenotyping under field conditions have been phenotyped with two main approaches, namely, excavation followed by imaging, also referred as shovelomics (reviewed in Joshi et al., 2022; Lynch, 2022; Nehe et al., 2021) and soil core-breaking methods (reviewed in Ober et al., 2021; Zhang et al., 2020), both labor- and cost-intensive methods. Based on these phenotyping bottlenecks, high-throughput phenotyping platforms (HTPPs) dedicated to RSA investigation (Nagel et al., 2012; Nakhforoosh et al., 2021; Poorter et al., 2023) have been developed, including automated rhizotrons and rhizotubes. HTPPs have the potential to allocate a larger number of individuals and allow deeper phenotyping of seminal and adult root systems (Colombo et al., 2022; H. Liu et al., 2021; Nakhforoosh et al., 2021), also in time-course experiments (Parasurama et al., 2023).

One of the advantages of HTPP approaches is that they allow wider populations or germplasm collections to be screened at higher detail levels, thus enabling accurate genome-wide linkage and association mapping (GWAS) studies (Atkinson et al., 2019; Singh et al., 2019; Tardieu et al., 2017). HTPPs are therefore technologies relevant for increasing traits' heritability (Tuberosa, 2012) and performing non-destructive, accurate root system observations as required for GWAS. Once the loci and alleles controlling the beneficial RSA traits are identified, selection efficiency can be improved by molecular tools, in particular molecular markers tightly associated to loci/alleles controlling proxy root traits directly related to a more complex target phenotype (e.g., RGA, final root length density distribution, related to drought tolerance). In individuals and populations, native nucleotide variants (including single nucleotide polymorphism [SNP] and INDEL [INsertion-DELetion) at nucleotide level) are organized in chromosomal haplotypes (Kimura & Crow, 1964). Molecular haplotypes, particularly gene-based haplotypes, are the functional units ultimately underlying phenotypic traits and alleles (Rafalski, 2002). Additionally, long-range and genic haplotypes are inherited through generations and are continuously subjected to recombination. Haplotypes, differently from single SNP, can be traced in pedigrees and in populations based on the identity-by-descent theory (Zhou

Core Ideas

- Root system architecture (RSA) and shoot-to-root biomass allocation are key for efficient crop use of water and nutrients.
- Knowledge on the genetic control underlying the RSA QTLome is limited and accurate dissection is challenging.
- GROWSCREEN-Rhizo was used to phenotype a worldwide panel of 194 elite durum wheat accessions for 35 traits.
- GWAS detected 39 multi-trait quantitative trait locus (QTL) clusters, including 10, 11, and 10 for seminal, nodal, and lateral roots, respectively.
- Single nucleotide polymorphism (SNP) haplotype distribution showed contrasting selection patterns in rainfed and irrigated breeding programs.

et al., 2020). Therefore, haplotype-based genome-wide association mapping, haplotype-based genetic dissection of QTL effects, and downstream haplotype-based breeding applications such as marker assisted selection and genomic selection are considered among the most advanced tools currently available to molecularly informed breeders (Bath et al., 2021; Langridge et al., 2022; Maccaferri et al., 2022).

In this study, we investigated root and shoot growth in rhizoboxes at a developmental stage previously unexplored in wheat GWAS studies. The experiment enabled the assessment of phenotypic variation and inheritance of seminal, adventitious, and lateral root development in elite DW cultivars and advanced lines from globally. We genetically characterized the panel using the Illumina *iSelect* 90K wheat SNP array (Wang et al., 2014). The study evaluated constitutive carbon partitioning based on above- and below-ground biomass. Additionally, this study investigated the co-location between QTL for different root and shoot traits using the "QTL cluster" approach with the aim of deciphering and, possibly, discriminating between pleiotropy, at both shoot and root levels, versus independency of factors affecting the plant growth. In conclusion, the analysis of QTL haplotype segregation within population structure groups enabled us to infer the selective pressure favoring RSA alleles over successive breeding and selection cycles.

2 | MATERIALS AND METHODS

2.1 | Plant material and experimental design

The population included a total of 194 DW cultivars from Italy, Spain, Morocco, Tunisia, Southern United States, CIMMYT (International Maize and Wheat Improvement Center), and ICARDA (International Center for Agricultural Research in the Dry Areas) selected to (i) evenly represent genetic diversity of the elite DW germplasm and (ii) limit heading date variation within a 10-day window in Mediterranean environments. The 194 cultivars were thoroughly genotyped with simple sequence repeats (SSRs), DArTs (Diversity Array Technology(R) markers; Maccaferri et al., 2011) and, later, with the Illumina *iSelect* 90K wheat SNPs array (Wang et al., 2014). The genetic position of the markers was assessed according to a DW consensus map constructed using the same genotyping technology (Maccaferri et al., 2015) and the reference DW Svevo genome assembly v1.0 (Maccaferri et al., 2019). Importantly, the same genetic material was characterized for grain yield, yield components, and other phenological and morpho-physiological traits in 16 field trials throughout different locations of the Mediterranean basin (Maccaferri et al., 2011).

The UNIBO (University of Bologna) association durum panel (UNIBO-DP) was previously characterized for RSA and shoot traits at the seedling stage (Canè et al., 2014; Maccaferri et al., 2016). Population structure of the panel phenotyped in the rhizoboxes consisted of five main groups representing the main breeding lineages detectable in the DW elite germplasm. These main groups corresponded to *ICARDA_dry*, ICARDA, and Italian accessions for dryland areas from the native Syrian and North African germplasm; *ICARDA_temp*, ICARDA accessions bred for temperate areas; *Italian*, with cultivars related to "Valnova" and "Creso" founders and subsequently bred with CIMMYT and Southwestern US accessions (Desert Durum); *CIMMYT_70*, widely adapted early CIMMYT germplasm introduced to several Mediterranean countries ("Yavaros_C79" CIMMYT founder, released as Karim in North Africa and Latino and Duilio in Italy; *CIMMYT_80*, more recent high-yield-potential CIMMYT germplasm ("Altar_C84" founder). Details are reported in Maccaferri et al. (2011). Additional main lineages related to the *North American* and *French* germplasm were removed from the experiment though present in the UNIBO-DP because of a strong population structure effect on phenology, which acts as a confounding side effect, related to a differential partitioning of *Ppd-A1* and *Ppd-B1* photoperiod-sensitive alleles.

To screen the entire population, three distinct sub-experiments were carried out. Four plants of two different cultivars were transplanted in each rhizobox (see below) and each cultivar was replicated in two different rhizoboxs for a total of four plants per cultivar. The most representative lines of the five population structure groups were replicated in the three sub-experiments as control lines. Thus, 63 accessions and five checks were screened in each of the three sub-experiments. The 63 accessions were chosen to uniformly sample the genetic diversity evidenced by population structure. Within each of the main population structure groups, accessions were randomly sampled and assigned to each of the three sub-experiments.

2.2 | Growing conditions and phenotyping

For each accession, healthy seeds with uniform size were pre-germinated on filter paper into individual Petri dishes. To guarantee germination uniformity, seeds were allowed to pre-germinate in dark and cold rooms (4°C) for a week. After pre-germination, uniform and vital seedlings were transplanted into the rhizoboxes. Rhizoboxes were filled with ≈18 L of dark and nutrient-rich peat-based compost. Each rhizobox was watered twice per day using 100 mL of water. Plants were allowed to grow for 4–5 weeks after transplanting up to the stage at which the longest roots reached the bottom of the rhizoboxes (corresponding to the Zadock scale 16, on average).

FIGURE 1 GROWSCREEN-Rhizo rhizoboxes and wheat genotypes in the high-throughput phenotyping platform (HTPP).

Plants were grown in the GROWSCREEN-Rhizo phenotyping facility at the IBG-2: Plant Science Institute, Forschungszentrum Jülich, Germany. A detailed description of the platform is presented in Nagel et al. (2012). Briefly, GROWSCREEN-Rhizo comprises two rows of 36 frames, totaling 72 slots where peat-filled "rhizoboxes" (90 cm × 70 cm × 5 cm) are inserted (Figure 1). Rhizoboxes are parallelepipeds measuring 90 cm × 70 cm × 5 cm, with one of their primary surfaces constructed from transparent plastic, facilitating the dynamic assessment of the root system. The entire structure is placed in the Phytec Greenhouse at IBG-2 Plant Science. Images of the rhizoboxes were collected with an automated imaging cabinet. Given the relatively large size and depth of the rhizoboxes, plants were grown up to the full tillering stage (Zadock Z29-30) before the deepest roots reached the bottom of the rhizobox (Gioia et al., 2015). Plants were allowed to grow for 5 weeks after transplanting, corresponding to the Z25, on average. Plants were grown under semi-controlled conditions, with a 16/8 h light/dark photoperiod (400 microEinstein per m^2 on average at plant level) with day/night temperatures of 24/18°C. Linear measurements of leaf length and width were collected twice a week in the first 2 weeks of growth and once a week in the following 2 weeks of the experiment. In parallel to shoot phenotyping, images of the root system were collected and length of seminal, lateral, and nodal roots, as well as root system distribution by soil depth parameters, were obtained using *GrowScreen Root* software (Nagel et al., 2012). Dynamic traits were estimated from the joint analysis of all measurements collected throughout the experiment. Leaf chlorophyll content was estimated twice using the SPAD (chlorophyll content)-502 chlorophyll meter (Minolta Corp.) at the Z14 and Z15 growth stages. Shoot dry weight (SDW) was measured after drying the tissues for 4 days at 65°C. Roots were collected and stored at 4°C in water at the end of the experiment. After accurate washing and removal of substrate particles, roots were dried in an oven at 65°C for at least 4 days and subsequently weighed. Simple traits were collected for the sake of dissection of complex traits, thus improving genetic association power. The conceptual dissection of the most complex trait measured in this experiment (root and shoot dry weight [RSDW]) into traits of progressively lower level of complexity is reported in Figure 2.

Traits measured in this experiment are grouped in final-point and dynamic. Final-point traits were either collected the day before harvest or in the next few days. Dynamic traits were estimated from the joint evaluation of all the measurements collected during the experiment. Simple traits were collected for the sake of dissection of complex traits, thus improving genetic association power. In Figure 2, we report the conceptual dissection of the most complex trait measured in this experiment (RSDW) into simpler traits. Leaf area (SLA) was scored by manually measuring the length (SLL) and the maximum width (SLW) of each leaf of the plants. SLA per each leaf was then calculated according to the well-known formula given as follows (Kemp, 1960; Masle & Passioura, 1987):

$$SLA = SLL \times SLW \times 0.858$$

Tiller and leaf counts were performed as well. These measurements were taken twice a week in the first 2 weeks of growth and once a week in the last weeks of the experiment as well as the day before harvesting. The root system was separated from the shoot at ground level at the end of the experiment. Shoot fresh weight was assessed at harvest, while SDW was measured after drying the tissues for 4 days at 65°C. Roots were collected and stored at 4°C in water at harvest. After an accurate cleaning of root systems from residuals of compost, roots were dried in an oven at 65°C for at least 4 days and weighed.

Pictures of the visible root system were taken daily but we analyzed only those pictures taken the same days when shoots were phenotyped. Images of the root system were analyzed by the software GrowScreen Root (Nagel et al., 2012). Briefly, GrowScreen Root allows to digitally draw the root system, distinguishing the three different root classes. We classified roots as seminal, nodal, and lateral. The outputs provided by the software are root length for each root class, maximum depth and width of the root system, and root length density for each chosen root class at different depths.

Dynamic traits have been calculated from the joint evaluation of data from all the phenotyping sessions carried out during the experiment. Growth curves for leaf area expansion, total root system elongation, and root system depth were fitted using Gompertz's growth curve as a model (Gompertz, 1825). Briefly, Gompertz's growth curve is a special logistic curve asymmetrical around the flex point. The characteristic parameters of Gompertz's curves are lag phase duration (lambda, λ), maximum growth rate (mu, μ), inflection point time (t0), and upper asymptote (A0). We extrapolated from

growth curves the maximum leaf expansion rate (μ-SLA), the maximum root elongation rate (μ-rlen), maximum root deepening rate (μ-dep), and day of root deepening inflection point (t0-dep).

The reported root density traits were referred to the day before harvest.

Leaf chlorophyll content was estimated twice using the SPAD-502 chlorophyll meter (Minolta Corp.) at stages Z13 and Z14 of the Zadok scale. A summary of the mean, range, repeatability, and description of the evaluated traits is reported in Table 1.

2.3 | Data analysis

Data analysis was carried out using the R statistical software (The R Core Team, 2016). Since phenotype distributions were not always normal (Figure S1), all data were transformed using the quantile normalization technique (Hicks et al., 2017).

Mean cultivar repeatability (h^2) was calculated using the following formula:

$$h^2 = \frac{{\sigma_g}^2}{{\sigma_g}^2 + \frac{{\sigma_e}^2}{r}}$$

where σ_g is the genetic variance; σ_e is the residual variance; r is the number of replicates, four in this study.

Data for heritability evaluation were first corrected for the sub-experiment effect. To remove the effects due to the subsequent sub-experiments and spatial variation, best linear unbiased estimates (BLUEs) were calculated using the line ID as fixed effect while sub-experiments and spatial variables were considered as random effect variables. The mixed models were fitted using the lme4 R package (Bates et al., 2015).

2.4 | Linkage disequilibrium decay analysis and population genetics

We fitted the SNP decay curve according to Rexroad and Vallejo (2009) and Sved (1971), who based the analysis on the known relationship between linkage disequilibrium (LD) as measured by R^2 (squared correlation of allele frequencies at a pair of loci) and effective population size N_e.

$$E\left(r^2\right) = \frac{1}{\alpha + kN_e c} + \frac{1}{n}$$

where c is the recombination rate between loci and n is the experimental sample size. In the absence of mutation, the constant α was set to 1 (Sved, 1971). The constant k was set to 4 for autosomes. Knowing R^2 LD values and c, we estimated N_e by fitting this nonlinear regression model:

$$y_{ij} = \frac{1}{\alpha_j + \beta_j + c_{ij}} + e_{ij}$$

where $y_{ij} = r^2 - 1/n$ is the observed LD (adjusted for chromosome sample size n) for marker pair i in chromosome j, and c_{ij} is the recombination rate from two-point linkage analysis for marker pair i in chromosome j. The parameter β_j is the estimator of effective population size for chromosome j, where

$$\hat{N}_e = \frac{B_J}{k}$$

The parameters α_j and β_j were estimated iteratively by using nonlinear modeling.

The decline of LD with distance (recombination rate in Morgans) was estimated by fitting the nonlinear regression model again

$$y_{ij} = \frac{1}{1 + kb_j + d_{ij}} + e_{ij}$$

where $y_{ij} = r^2 - 1/n$ is the observed LD between markers, the constant $k = 4$ for autosomes, d_{ij} is the recombination rate from two-point linkage analysis for marker pair i in chromosome j, bj is the estimate of effective population size for chromosome j, and e_{ij} is a random residual. The estimates of R^2 for pairs of markers were adjusted for experimental sample size.

To assess the significance threshold to include a marker in the QTL model, we first calculated the upper LD threshold for the background LD caused by population structure by inspecting the distribution of LD values for unlinked marker pairs (>50 cM genetic distance in the consensus maps) and by selecting as threshold the R^2 corresponding to the 95th percentile distribution. This R^2 value was used to spot, through the tagger function in the software Haploview (Barrett et al., 2005), a set of fully unlinked tag SNPs.

Population structure was estimated on the basis of the microsatellite and DaRT markers profile using the software Structure 2.3.4 (Pritchard et al., 2000). Kinship matrix was estimated as IBS on the basis of SSR markers.

2.5 | Genome-wide association study

Multi-locus mixed-model (MLMM) algorithm as implemented into the "mlmm" package (Segura et al., 2012) was used for phenotype/genotype association using both the kinship and population structure matrices as covariates. Briefly, this algorithm performs, in a first step, single-marker mixed-

TABLE 1 Description, minimum, mean, maximum "nominal values" and heritability regarding the shoot and root traits measured in the rhizobox experiment performed on the UNIBO elite durum panel from worldwide.

Phenotype	Description	Min	Mean	Max	h^2
End-point phenotypes					
Complexity level: I					
RSDW	Shoot and roots dry weight (g)	0.03	0.41	1.02	0.48
Complexity level: II					
SDW	Shoot dry weight (g)	0.30	0.56	0.91	0.48
RDW	Root dry weight (g)	0.04	0.06	0.11	0.56
SRR	Shoot/root ratio (g/g)	0.54	7.34	17.68	0.60
Complexity level: III					
SLA	Leaf area (cm^2)	22.87	99.51	204.84	0.64
SLSW	Leaf specific weight (g/m^2)	9.47	35.82	62.22	0.35
RTL	Total root length (cm)	80.96	331.03	833.34	0.60
RSW	Root specific weight (g/m)	0.005	0.016	0.077	0.43
Complexity level: IV					
SLN	Total leaf number (nb)	6	16.94	37	0.44
SALA	Average leaf area (cm^2/leaf)	1.99	5.98	13.5	0.71
RSL	Seminal root length (cm)	50.0	246.4	555.0	0.47
RNL	Nodal root length (cm)	0.00	61.75	366.67	0.63
RLL	lateral root length (cm)	0.00	23.13	187.85	0.68
RNS	Nodal/seminal ratio (cm/cm)	0.00	0.26	2.36	0.58
Complexity level: V					
STN	Tiller number (no.)	1.0	5.3	11.0	0.49
SLT	Average leaf number per tiller (no.)	5.0	7.2	12.5	0.85
SALL	Average leaf length (cm)	7.2	12.9	17.7	0.77
SALW	Average leaf width (cm)	0.27	0.44	0.60	0.76
Deep rooting traits					
RW	Root system width (cm)	5.51	16.46	55.26	0.48
RD	Root system depth (cm)	34.09	61.91	75.91	0.65
RD75	Depth of the 75° percentile of total roots (cm)	17.03	36.35	58.67	0.66
RTT	Density of roots above 35 cm ($cm \setminus cm^2$)	0.1	0.42	1.12	0.62
RST	Density of seminal roots above 35 cm ($cm \setminus cm^2$)	0.03	0.27	0.58	0.42
RNT	Density of nodal roots above 35 cm ($cm \setminus cm^2$)	0	0.13	0.69	0.62
RLT	Density of lateral roots above 35 cm ($cm \setminus cm^2$)	0	0.02	0.2	0.6
RTD	Density of roots below 35 cm ($cm \setminus cm^2$)	0	0.16	0.52	0.63
RSD	Density of seminal roots below 35 cm ($cm \setminus cm^2$)	0	0.15	0.44	0.61
RND	Density of nodal roots below 35 cm ($cm \setminus cm^2$)	0	0.003	0.096	0.31
RLD	Density of lateral roots below 35 cm ($cm \setminus cm^2$)	0	0.02	0.24	0.71
RMDD	Depth of maximum density of the root system (cm)	5.68	17.56	70.02	0.42
Dynamic traits					
RMDR	Maximum root deepening rate (cm/day)	1.45	3.5	6.3	0.47
RMGR	Maximum root growth rate (cm/day)	2.74	14.34	30.44	0.43
RDFP	Flex point of the deepening curve (day)	2.24	6.05	15.8	0.58
SMLER	Maximum leaf expansion rate (cm^2/day)	1.18	8.6	183.15	0.58

(Continues)

TABLE 1 (Continued)

Phenotype	Description	Min	Mean	Max	h^2
Other trait					
SPAD	Chlorophyll content	23.92	36.4	50.15	0.74

Note: Root and shoot biometric traits measured in the rhizobox experiment are dissected and reported based on their categorization into five "complexity levels," an empirical classification taking into account the developmental timeframe, the segmentation of the complex traits into their components corresponding to different organs, and the related genetic control of traits and sub-traits, which can range from pleiotropy to almost complete independence. Traits are categorized as: Complexity Level I, corresponding to the highest complexity, e.g., whole plant biomass; Complexity II, divides between shoot and root biomass; Complexity III, divides between the area/length and specific weight; Complexity IV, addresses leaf number at the shoot level and divides between seminal, nodal, and lateral root types; Complexity V, address tiller number, leaf length, and wide at the shoot level, and parameters to estimate the root depth distribution.

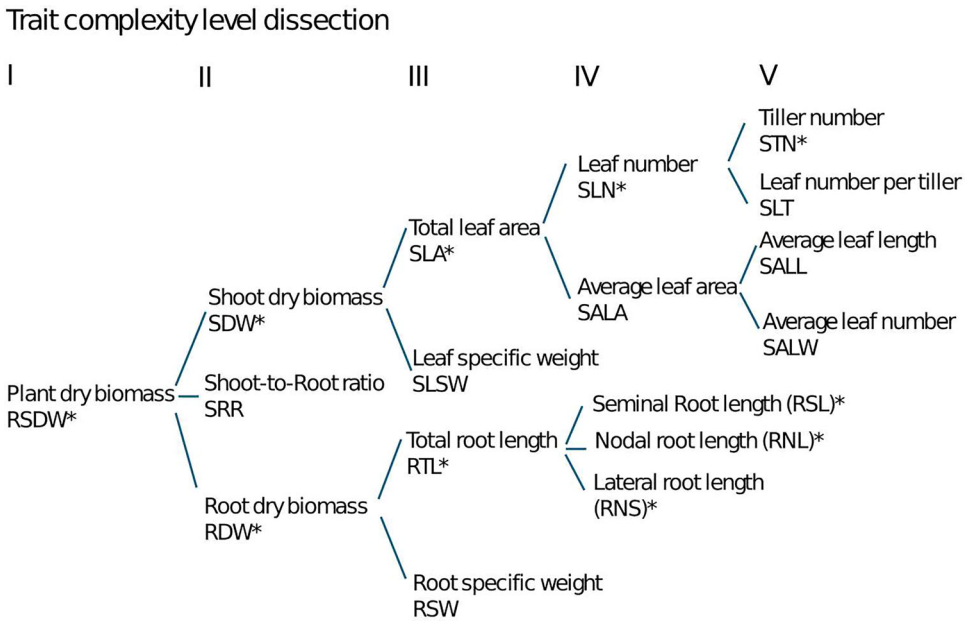

FIGURE 2 Conceptual dissection of the most complex trait measured in this experiment into simpler traits. Traits marked with an asterisk (*) have been directly measured while the other have been derived by calculation.

model association tests between phenotypic and genotypic scores using population structure and kinship as covariates. In the second step, those markers having the association *p*-value lower than a defined threshold are used to fit a global model including all the significant markers plus population structure and kinship. The global fit allowed us to exclude completely or partially redundant markers, maintaining in the model only the most informative markers. In the next steps, the procedure is repeated except that the global model found in the second step is used as covariate. This allowed us to account for the masking effect that major effect loci might have on minor QTL. The procedure is interrupted when no improvement is made in terms of explained heritability. Significance threshold for phenotype/genotype association was adjusted using the Bonferroni correction for multiple independent tests (Bonferroni, 1936). The number of independent tests was set equal to the number of independent SNPs. Bonferroni correction for multiple tests on the MLMM was applied to allow the algorithm to account for marker effects in the GWAS–QTL model. Confidence intervals (CIs) were assessed by inferring the genetic distance where, on average, LD decayed to R^2 value ≤ 0.3. The tag markers associated with phenotypes falling within the same CI were considered and discussed as belonging to a unique QTL cluster. We also reported those QTLs with a significance *p*-value higher than the genome-wide threshold but lower than 0.001 considering them as putative QTL (Maccaferri et al., 2016). QTL effect direction was reported according to the +/− sign of the allelic effect of the QTL, which showed higher average LD with other markers of the same cluster. QTL effects are reported as a percentage of the mean population value.

Haplotypes were computed using the LD spline algorithm (Bush et al., 2009) implemented in the Haploview software (Barrett et al., 2005). We used the following setup to obtain a number of haploblocks compatible with what was expected from LD decay study: blockCutHighCI = 0.98, blockCutLowCI = 0.7, blockRecHighCI = 0.7. To ensure the evaluation focused on well-represented, non-rare haplotypes, those with a frequency of less than 5% were excluded from further analysis, in accordance with standard and widely

accepted GWAS methodology. To assess haplotype relationships, we first computed the genetic distances using the function "dist.dna" of the R package "ape" (Paradis & Schliep, 2018); in a second step, we grouped the haplotypes according to the Ward's criteria implemented in the function "hclust" from the fastcluster R package (Müllner et al., 2013).

To assess the relevance of each locus in defining the population structure, we computed discriminant analysis of principal component (DAPC) using the "adegenet" package (Jombart, 2008). We chose to consider the number of principal components as necessary to explain 90% of the genetic variance. This resulted in a Baesian information criterion of the grouping minimized between five and six clusters. We choose to group accessions in five clusters to reflect the breeding and environmental history of the panel and previous literature references. For the first three principal components of genetic diversity, the calculated marker loadings of each PC were standardized based on the maximum observed value of the given PC. Significance was established as 95, 99, and 99.9 quantiles of the standardized marker loadings for each PC.

2.6 | Candidate gene analysis, GO enrichment, and gene network exploration

The *T. turgidum* 'Svevo' genetic intervals of QTL clusters *QCls3.ubo-1B*, *QCls25.ubo-6A*, and *QCls32.ubo-7A* were explored looking for candidate genes, gene ontology (GO) terms, and enrichment and gene networks involved in root morphology, development, and RSA. The QTL clusters' genetic intervals were explored from the Ensembl plant database (Dyer et al., 2024) using *T. turgidum* 'Svevo' as reference genome (Maccaferri et al., 2019), collecting information about gene function description, GO terms, and gene orthologues in *Arabidopsis thaliana*, *T. aestivum* 'Chinese Spring' RefSeq v1.1 (The International Wheat Genome Sequencing Consortium (IWGSC) et al., 2018) and *Triticum dicoccoides* 'Zavitan' v1.0 (Avni et al., 2017), as well as paralog and homoeologue genes from Svevo genome. Furthermore, the GO enrichment was performed on the same genetic interval from the three main QTL clusters separately, using *gProfiler* tool (Raudvere et al., 2019). Basically, GO terms were divided in molecular function (MF), biological process (BP), and cellular compartment (CC) and filtered for GO terms with a statistically significant association p-value < 0.05. Results were then plotted using a custom R script with *dplyr* (Wickham et al., 2022) and *ggplot2* (Wickham et al., 2025) packages.

Further candidate gene characterization was performed exploring gene networks associated with root development, morphology, and RSA. In order to restrict the CI, a genetic region corresponding to ±1 Mb from the GWAS Tag SNP of each QTL cluster (*QCls3.ubo-1B*, *QCls25.ubo-6A*, and *QCls32.ubo-7A*) was considered. For each interval, the orthologue genes of *T. aestivum* 'Chinese Spring' RefSeq v1.1 collected from Ensembl plant database were used in Knetminer software (Hassani-Pak et al., 2021). The gene networks were obtained and filtered for correspondence to root morphology, development, and RSA, retaining the significantly associated networks with $p < 0.05$. In order to further characterize the QTL cluster intervals and the gene functions, a transcriptomic atlas exploration was performed on *T. aestivum*, *A. thaliana*, and *Oryza sativa* subsp. *japonica* species orthologue genes. The *A. thaliana* and *O. sativa* subsp. *japonica* orthologues were filtered for the alignment coverage higher than 0 to select only the most reliable orthologue genes. The following expression atlas was explored for each species: exVIP for *T. aestivum* (Borrill et al., 2016; Ramírez-González et al., 2018), and EMBL expression atlas for *A. thaliana* and *O. sativa* subsp. *Japonica* (Moreno et al., 2022). From each expression atlas, leaf, shoot, and root tissues at seedling and adult plant stages were explored and expression values were extracted in transcript per million normalization values.

3 | RESULTS

3.1 | Root and shoot trait variation, heritability, and correlations

In total, 35 root and shoot traits were measured and adjusted BLUEs were subsequently subjected to GWA analysis (Table 1), with traits decomposed by four hierarchic biological and genetic complexity levels, from the most complex—total plant biomass, Level I—down to the single shoot and root components—Level IV and V. A wide range of variation was observed for most of the traits as well as for each of the three main root classes (seminal, nodal, and lateral). Repeatability, reported as h^2, ranged from 0.31 to 0.85 for length of visible nodal roots below 35 cm and average leaf number per tiller, respectively.

At the end of the experiments (growth stage Z31), the seminal root apparatus extended in rhizoboxes through most of the allowed vertical space (maximum root system depth from 34.1 to 75.9 cm), while the nodal roots were mostly confined to the top 35-cm layer. Considering the final length of the three root classes, the seminal root apparatus reached a maximum of 555.0 cm/plant compared to a maximum of 366.7 and 187.8 cm for the nodal and lateral roots, respectively. Total root system width showed a wide range of variation, from very narrow (5.0 cm) to wide root systems (up to 55.3 cm). Root dry weight ranged from 0.04 to 0.11 g/plant.

In total, 11 static and three dynamic root traits directly or indirectly (proxies) related to the deep rooting complex trait were considered (Table 1). In addition to the simple root system depth, we considered traits potentially related to the

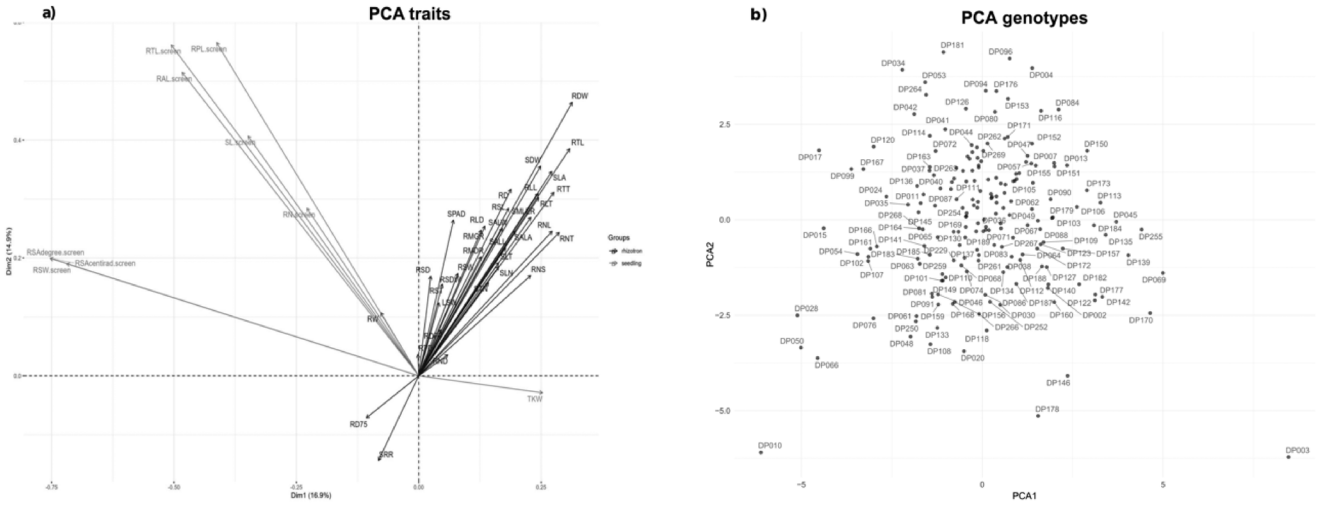

FIGURE 3 Principal component analysis (PCA) biplot graphs of shoot and root traits measured in the rhizobox and paper-sheet experiments and genotypes of the UNIBO elite durum panel from worldwide. 3A reports PC1–PC2 dimensions; 3B reports PC1 and PC2 dimensions of genotypes; acronyms and arrows for rhizobox traits (this study) are reported in black font while those for paper-sheet experiments (Canè et al., 2014) are reported in gray font.

capacity of the crop to extract water from the deep layers, specifically depth of the 75th percentile of total roots, root density in the deep layers (below 35 cm, for the total apparatus and for the seminal, nodal, and lateral roots, respectively), and total root system width. Root density was recorded for both shallow (<35 cm) and deep soil layers (>35 cm) as well as for the seminal, nodal, and lateral root systems separately.

Among the dynamic traits considered as proxies for deep rooting, the maximum root deepening rate (or maximum root elongation rate) varied between a minimum of 1.45–6.30 cm/day, while the day of deepening point varied between 2.24 and 15.8 days after germination. The root maximum elongation rate varied consistently from 2.74 to 30.44 cm/day.

The shoot-to-root ratio ranged from 0.54 to 17.68 with an h^2 value of 0.60. The shoot development in terms of biomass at the end of the growth cycle varied considerably among accessions (from 0.30 to 0.91 g/plant), concomitantly with final tiller number (TN) (from 1 to 11 tillers/plant).

Shoot and root trait distribution approached the normal distribution in most cases (Figure S1). However, several nodal and lateral root traits (namely, lateral root length, nodal root length, maximum nodal root density, maximum lateral root density, and root system width) showed positively skewed distributions.

3.2 | Traits from seminal, nodal, and lateral root classes showed limited correlations

Principal coordinate analysis (PCA) biplot graphs and single genotypes among rhizobox and paper-screen traits are reported in Figure 3.

PCA showed clearly that (i) root traits from the two rhizobox and seedling paper-screen methods are highly distinct, as expected to some extent, (ii) RGA traits as measured on seedling roots in paper-screen are more related to the root system width (RW) among the traits related to deep rooting observed in rhizoboxes, (iii) traits observed in rhizoboxes did not cluster into clearly distinct subgroups indicating a relatively low degree of correlation among single traits. Shoot-to-root ratio, depth of the 75th percentile of total roots, and root system width were the most distinct traits among the others (Figure 3a).

The correlogram (Figure S2) confirmed PCA preliminary indications. More in detail, seminal, nodal, and total lateral root length were poorly correlated to each other (seminal length vs. nodal length, $r = 0.17$*; seminal length vs. lateral length, $r = 0.29$***; nodal length vs. lateral length, $r = 0.27$***), indicating that the inheritance of the three root types is only moderately related. Shoot and root dry weight were strongly correlated at $r = 0.74$***, indicating a partial common inheritance for the two traits, as expected. Shoot-to-root ratio was significantly correlated with root dry weight but not with SDW ($r = -0.53$*** and 0.15, respectively). Nodal root length was positively correlated with TN ($r = 0.38$***) and other shoot traits. Maximum root density depth and depth of the 75th percentile of roots showed stronger correlation with nodal root traits, underlining the importance of these root classes in shaping root spatial distribution. Among root dynamic traits, maximum deepening rate and maximum elongation rate correlated positively and highly significantly (r from 0.40 to 0.85) with total root length, root dry weight, maximum root depth, seminal root at depth, and total roots at top. These results indicate that both root growth dynamic traits

could be considered good proxies for root end-point traits related to total root system development and depth, thus allowing the development of models able to estimate these traits at an earlier growth stage (i.e., within 21 days after germination) in defined environmental conditions.

Based on the availability of RSA data quickly assessed at the seedling stage in filter paper sheets on the same panel (Canè et al., 2014), the pattern of correlations between the traits obtained in the paper sheet and rhizobox experiments was assessed (Figure S2). The seedling root system angle assessed in paper sheet (RSW-screen [root seedling width], RSA-screen) showed highly significant positive correlations with the root system width of adult plants in rhizoboxes ($r = 0.37$***) and negative correlations with total root length, nodal and lateral total root length ($r = -0.15, -0.20$). Additionally, the seminal root number at the seedling stage showed a moderate positive highly significant correlation with both root density (RTT) in rhizoboxes and depth of the 75th percentile of total roots (RD75) at the adult stage ($r = 0.24$ and 0.27, respectively).

3.3 | Shoot and root traits have been differently shaped by breeding programs conducted in relation to environments

Figure 4 reports the biplot of the first two PCs and *k-means* grouping of population structure as computed by the DAPC (Jombart et al., 2010). Figure 4 reports the loading coefficients of the first three PCs for all the markers. Red lines indicate markers with loadings in the top 1%, indicative of chromosome regions with SNP showing the highest correlations to the overall germplasm population structure. Genetic relationships among cultivars and breeding lines defined five groups of cultivars/lines, whose root and shoot phenotypic differences correlated to population structure, mainly corresponding to known breeding lineages. Table S1 reports Tukey's least significant difference grouping of the five subpopulations for all traits. As to root classes, seminal root traits showed high differentiations among the most important subpopulations/breeding programs, while no differences between subpopulations were observed for lateral root traits. Nodal root differentiation was observed between *Italian* and *ICARDA_temp* subpopulations for nodal root density below 35 cm. Overall, *Italian*, *ICARDA-dry* and *ICARDA-temp* subpopulations showed a root-oriented and deep-rooting behavior, resulting in the top subpopulations for root depth, seminal and nodal density at depth, and total root length. Moreover, the accessions of these three subpopulations showed negatively skewed root system width values, indicating a higher than average frequency of accessions with longer and geotropic root systems. Remarkably, the *Italian* subpopulation showed among the lowest shoot-to-root ratio and root-specific weight. Conversely, the *CIMMYT_80* subpopulation showed a markedly shoot-oriented carbon partitioning, being by far the subpopulation with the highest shoot-to-root ratio, SDW, SPAD, and leaf-specific weight. In addition to this, all *CIMMYT_80* accessions were consistently classified as top-ranking for positively skewed root system width values, indicating a prevalence of shallow roots in this widely used subpopulation. Additionally to RW, the *CIMMYT_80* subpopulation showed the lower seminal and total root length, and value close to the average for root depth.

3.4 | Dissecting complex traits to simpler components allows for a more detailed characterization of their genetic architecture

A total of 180 QTL peaks were detected for the 35 analyzed traits, with an average of 5.14 QTLs per trait. Table S2 reports detailed metrics for each QTL detected in this experiment. Table 2 reports a summary of the QTL model results for the analyzed traits. For each phenotype, we report the R^2 of the global QTL model and minimum, mean, and maximum adjusted R^2 of the single QTL detected for each phenotype. Major QTLs with R^2 values exceeding 10% were detected for 28 out of 35 traits. Single QTL R^2 values ranged between 3.96% and 29.48% for nodal/seminal length ratio and average leaf width, respectively. Overall, a higher than average R^2 of the QTL models was detected for traits at a lower degree of complexity. A comparable trend was observed in terms of partial R^2 explained by a single QTL. Similarly, the number of QTL signals that reached significance was higher for simpler traits (Table 2). As an example, six QTLs were detected for total root length at Complexity Level III, while 10 QTLs in total were identified for the root length dissected into the three main root system components, namely, seminal, nodal, and lateral root length, at Complexity Level IV. Similarly, two QTLs were detected for leaf area, while up to five and eight QTLs were detected when leaf area was broken down into leaf number and average leaf area, which in turn when dissected into average leaf length and width, showed to be controlled by 14 and 13 QTLs, respectively.

3.5 | Co-localization of QTL suggests a mostly independent genetic basis for main root classes

We defined as major QTL clusters those chromosome regions showing co-location of three or more distinct single-trait QTLs, with overlapping supporting intervals. Thus, a total of 39 QTL clusters were detected in all chromosomes but 3B and 4A (Table 3; Figures 5 and 6) with 117 out of 180

TABLE 2 Cumulative variance accounted for by multi-quantitative trait locus (QTL) models regarding the shoot and root traits measured in the rhizobox experiment performed on the UNIBO elite durum panel. R^2 values are reported for the QTL model only (without population structure), for the population structure, and the global model including population structure and multi-QTL.

Trait	Multi-QTL R^2 (%)	Population structure R^2 (%)	Global R^2 (%)	Min QTL R^2 (%)	Mean QTL R^2 (%)	Max QTL R^2 (%)	QTL number (no.)
Complexity level I							
RSDW	16.79	1.71	22.28	6.34	8.76	11.21	3
Complexity level II							
SDW	17.44	1.76	23.09	5.96	9.12	11.82	3
RDW	15.6	0.28	18.13	2.3	3.85	4.93	4
SRR	29.01	0.51	30.58	6.57	9.54	11.36	5
Complexity level III							
SLA	14.1	1.00	15.5	9.46	9.97	10.47	2
SLSW	44.34	15.37	50.36	9.15	12.87	16.33	7
RTL	35.27	0.33	37.58	6.03	9.92	15.91	6
RSW	20.45	1.01	22.71	3.16	6.24	10.68	4
Complexity level IV							
SLN	31.26	0.88	33.06	6.62	9.68	15.55	5
SALA	45.91	1.31	53.37	9.91	14.57	21.79	8
RSL	23.59	1.78	24.91	6.78	9.73	14.64	3
RNL	15.03	2.14	13.84	5.06	6.47	8.83	3
RLL	24.5	0.77	29.89	7.34	10.09	16.34	4
RNS	16.21	2.04	15.04	3.46	3.75	3.96	4
Complexity level V							
STN	10.71	0.37	21.39	6.97	8.35	9.96	3
SLT	9.34	10.43	45.72	9.01	12.39	18.29	6
SALL	65.73	1.71	65.83	4.55	14.92	28.88	14
SALW	53.88	2.13	67.51	4.46	16.72	29.58	13
Root distribution/deep rooting traits							
RW	47.78	1.59	46.89	4.69	11.24	22.74	7
RD	20.58	6.98	25.92	5.04	7.76	13.1	3
RD75	23.11	1.94	23.62	7.07	9.06	13.22	4
RST	25.57	0.79	33.53	3.78	7.59	14.33	6
RNT	11.93	2.23	12.92	3.55	5.05	6.27	3
RLT	28.79	1.25	30.09	4.61	9.68	19.77	4
RSD	22.42	6.11	26.72	6.5	9.2	13.76	3
RND	22.88	1.94	22.84	2.28	5.36	13.06	5
RLD	51.34	0.07	54.29	6.88	11.74	16.22	10
RTT	19.47	0.74	30.96	6.25	10.55	13.21	5
RTD	35.13	4.26	38.96	3.38	8.62	17.82	6
Dynamic traits							
RMDR	32.97	3.01	37.98	4.69	9.38	13.46	6
RDFP	32.71	0.5	32.47	4.46	7.92	13.37	6
RMGR	16.47	0.51	15.46	6.79	8.84	10.88	2
SMLER	28.15	0.03	28.28	6.74	9.48	12.81	4
RMDD	19.38	2.73	19.88	6.13	7.60	10.35	3

(Continues)

TABLE 2 (Continued)

Trait	Multi-QTL R^2 (%)	Population structure R^2 (%)	Global R^2 (%)	Min QTL R^2 (%)	Mean QTL R^2 (%)	Max QTL R^2 (%)	QTL number (no.)
Chlorophyll-related traits							
SPAD	52.88	23.51	59.41	8.84	15.35	20.34	7

Note: RD, root depth (cm), whole root system; RD75, root depth, 75th percentile (cm), whole root system; RDFP, root deepening curve flex point (day), whole root system; RDW, root dry weight (g), whole root system; RLD, root dry weight (g), whole root system; RLL, root lateral length (cm), whole root system; RLT, density of nodal roots (cm/cm^2); RMDD, root maximum density, depth (cm), whole root system; RMDR, root maximum deepening rate (cm/day); RMGR, maximum root growth rate (cm/day); RND, root density in the deep layer, below 35 cm (cm$\smile$cm^2), nodal root system; RNL, root nodal length (cm), whole root system; RNS, root nodal-to-seminal ratio (cm/cm); RNT, density of nodal roots (cm/cm^2); RSD, root density in the deep layer, below 35 cm (cm$\smile$cm^2), seminal root system; RSL, root seminal length (cm), whole root system; RST, density of seminal roots (cm/cm^2); RSW, root seedling width; RTD, root density in the deep layer, below 35 cm (cm$\smile$cm^2), total root system; RTL, root total length (cm), total root system; RTT, density of total roots (cm/cm^2); RW, root system width (cm), total root system; SALA, shoot, average leaf area (cm^2); SALL, shoot, average leaf length (cm); SALW, shoot, average leaf width (cm); SLA, shoot, total leaf area (cm^2/leaf); SDW, shoot dry weight (g); SLN, shoot, leaf number per tiller (no.); SLSW, shoot, specific leaf weight (g/m^2); SLT, shoot, average leaf number per tiller (no.); SMLER, shoot, maximum leaf expansion rate (cm^2/day); SPAD, chlorophyll content; SRR, shoot-to-root ratio (g/g); STN, shoot, tiller number (no.).

QTLs found in clusters. Venn's diagrams in Figure 7a show the overlap between QTLs for root and shoot traits, as well as among QTLs for the three main root types (namely, seminal, nodal, and lateral roots) and shoot traits (Figure 7b). In 19 cases, QTL clusters included QTL for both root and shoot traits, indicative of major loci for whole plant vigor and architecture and/or major QTL affecting the shoot-to-root ratio. In total, we found 11 root-trait-specific QTL clusters

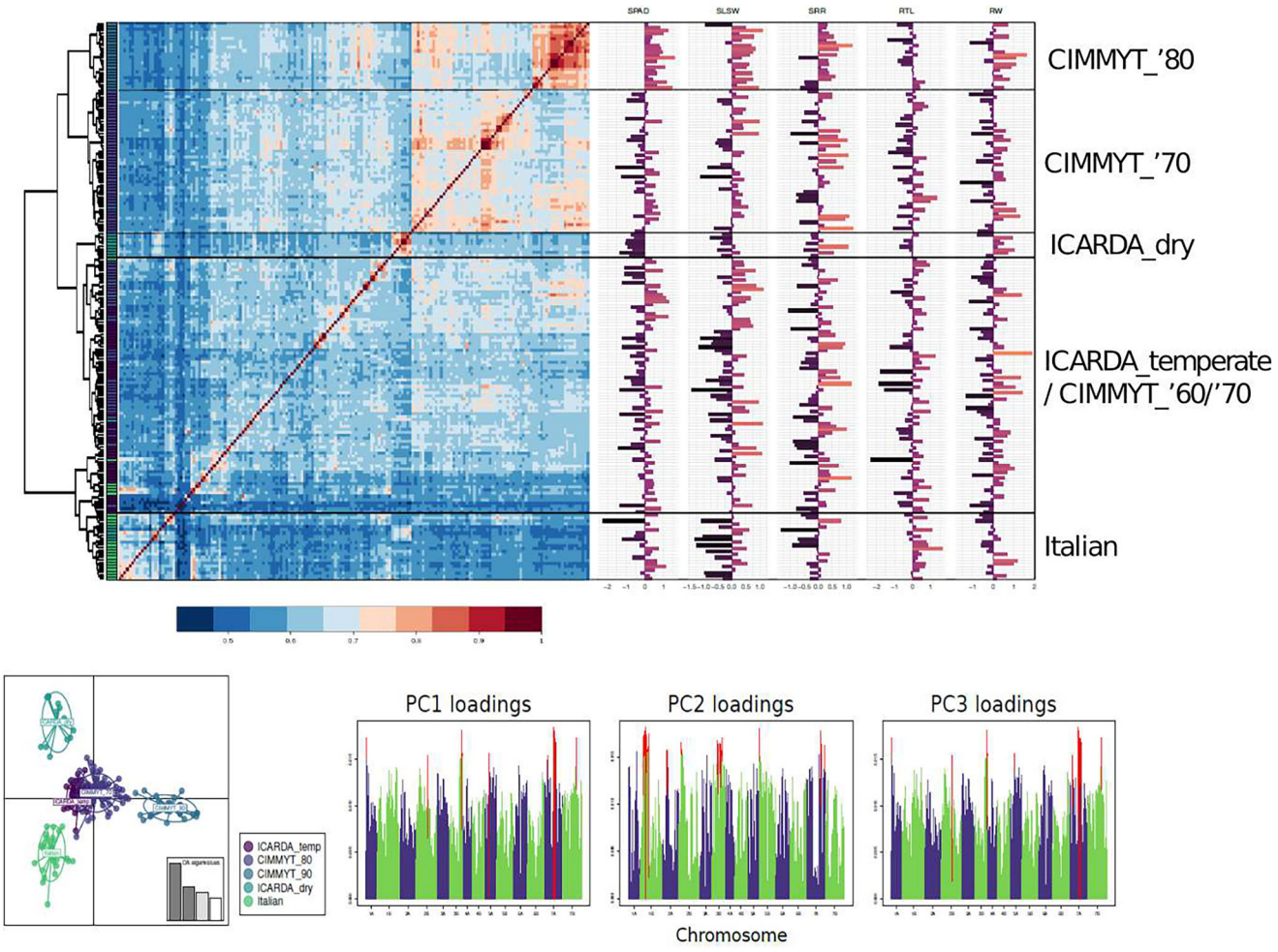

FIGURE 4 Graphical representation of population genetic structure in the durum wheat elite association panel and relationship between population structure and selected root and shoot trait. Distinct breeding lineages are identified by their origin/institution and decade.

TABLE 3 Quantitative trait locus (QTL) clusters for shoot and root traits from the HTP rhizobox experiment in the elite durum wheat panel. Acronym, single-trait QTL, tag-single nucleotide polymorphism (SNP) markers, confidence interval genetic and physical range and peak position in cM, QTL significance, effect, and R^2 range are reported for each QTL cluster.

QTL cluster (acronym)	Single component QTL (acronym)	Tag marker (SNP)	Chr. (no.)	QTL peak position (cM[a])	CI left (cM)	CI right (cM)	CI_peak (Mb[b])	CI left (Mb)	CI right (Mb)	-log$_{10}$(p) (range)	Effect range (%)	R^2 range (%)
QCls1ubo-1A	RD, RW, RSD, RTD, RTL	IWB35039	1A	75.1	72.2	84.5	488.75	482.49	504.76	3.2–4.1	11.8–17.3	5.0–7.3
QCls2ubo-1B	RNS, RNT	IWB59696	1B	3.0	0.3	6.1	4.93	4.07	9.57	3–3.4	5.9–6.9	3.7–5.4
QCls3ubo-1B	RDW, RLD, SDW, RDFP, RMGR, RTL, RSL, RSD, RTD, SALA	IWA7317	1B	82.2	75.6	90.1	553.13	492.24	578.04	3.1–7.2	5.7–14.3	3.4–19.3
QCls4ubo-1B	RLL, RLT	IWB72561	1B	140.1	137.1	143.5	652.91	651.46	656.16	5.8–7.4	14.5–18.2	16.3–19.8
QCls5ubo-2A	SALL, SLSW	IWB54406	2A	194.7	191.7	200.7	752.39	750.93	770.04	5.1–9.8	11.5–11.9	11.1–17.6
QCls6ubo-2A	SLN, RNS, SALL	IWA5978	2A	204.3	203.3	212.5	766.16	764.10	711.16	3.3–6.1	2.1–8.2	0.8–15.6
QCls7ubo-2B	RLD, RTT, RW	IWB28973	2B	12.2	8.4	21.2	16.24	9.99	25.05	4.5–6.4	10.5–11.7	9.4–11.1
QCls8ubo-2B	RD75, RMDR	IWB950	2B	76.6	73.7	81.7	158.79	139.18	163.97	3.0–4.7	9.6–13.3	7.1–11.4
QCls9ubo-2B	RST, SLSW	IWB68216	2B	108.2	100.5	112.3	514.70	446.14	537.61	3.1–5.9	10.7–18.8	3.8–12.9
QCls10ubo-2B	RST, RSL, RTD, SRR	IWB28961	2B	146.5	141.6	148	701.10	682.48	709.17	3.1–4.4	9.5–17.3	3.4–11.4
QCls11ubo-2B	RTD, RTL, RTT	IWB19170	2B	165.7	162.1	169.3	742.92	740.58	754.84	3.1–5.5	9.2–17.3	6.0–13.2
QCls12ubo-2B	SALA, SALL, SALW	IWB28826	2B	181.6	178.5	185.0	777.35	769.41	777.37	3.5–5.8	10.0–16.6	8.4–16.4
QCls13ubo-3A	RNL, RNS	IWB44601	3A	43.7	41.0	47.0	49.45	43.08	53.47	3.5–3.8	6.3–9.3	3.8–8.8
QCls14ubo-3A	SALW, SMLER	IWB48828	3A	49.9	46.9	53.7	62.77	53.47	97.53	3.2–4.1	7.7–9.7	6.7–12.2
QCls15ubo-3A	SDW, RSDW, RLD, SLSW	IWA1260	3A	105.3	97.2	108.3	600.29	594.41	717.73	4.3–7.4	7.9–17.4	9.2–16.3
QCls16ubo-3A	SLN, STN	wPt-3133	3A	123.5	121.8	127.7	662.16	654.28	674.01	4.1–4.4	7.8–9.2	7.9–8.1
QCls17ubo-4B	RLD, SALL, SMLER, SPAD	IWB11925	4B	34.4	23.5	37.4	35.05	23.30	41.57	3.0–6.1	8.1–11.8	4.6–12.6

(Continues)

TABLE 3 (Continued)

QTL cluster (acronym)	Single component QTL (acronym)	Tag marker (SNP)	Chr. (no.)	QTL peak position (cM[a])	CI left (cM)	CI right (cM)	CI_peak (Mb[b])	CI left (Mb)	CI right (Mb)	-log$_{10}$(p) (range)	Effect range (%)	R^2 range (%)
QCls18ubo-4B	RSW, RTD, RD	IWB1109	4B	83.1	77.2	86.8	614.48	585.29	627.67	3.4–3.8	10.6–12.6	3.2–5.4
QCls19ubo-5A	SALW, SLN	IWB50844	5A	14.3	11.6	19.9	8.76	7.80	11.74	3.1–10.8	7.9–22.3	6.6–29.6
QCls20ubo-5A	RNT, SALW	IWB71919	5A	67.3	64.2	77.2	405.26	400.33	421.14	3.1–3.3	5.7–6.7	4.5–6.3
QCls21ubo-5A	RTT, SLN	IWB25138	5A	146.5	143.5	149.7	554.32	547.14	559.34	4.0–4.1	9.1–12.6	6.3–7.9
QCls22ubo-5A	RLL, SALA	IWA3335	5A	199.6	193.3	203.3	644.74	639.31	647.97	3.3–8.0	16.7–24.4	7.5–21.8
QCls23ubo-5B	SPAD, SRR	IWB28778	5B	47.4	45.0	50.8	371.59	349.42	396.50	4.1–9.7	11.1–11.1	9.5–20.3
QCls24ubo-6A	RNL, RNT, SLSW	IWB30925	6A	62.1	59.1	66.3	492.67	462.88	517.72	3.2–7.0	5.2–16.3	3.6–15.2
QCls25ubo-6A	SLA, SALW, RDMD, RST, RW, RD75	IWB35245	6A	122.1	115.3	131.2	600.48	594.05	614.67	4.0–10.1	9.3–19.0	8.7–26.1
QCls26ubo-6B	SALL, SALW	IWB29294	6B	74.9	71.9	78.8	429.40	218.74	454.88	3.6–6.1	5.7–13.4	3.6–15.5
QCls27ubo-6B	SRR, SLN	IWB13090	6B	90.1	87.0	95.9	553.79	537.68	596.05	3.2–4.5	8.1–15.1	6.6–10.4
QCls28ubo-6B	RDW, SLA	IWB52925	6B	154.6	152.2	156.0	695.71	688.04	694.14	3.2–4.2	9.5–13.0	4.9–9.5
QCls29ubo-7A	SALL, SALW, SALA	IWB67175	7A	14.1	11.1	17.8	20.92	17.29	23.75	6.1–11.8	11.9–14.6	14.6–23.8
QCls30ubo-7A	RND, RSDW, SDW	IWB27639	7A	53.1	50.3	57.9	49.04	45.41	55.73	4.4–4.9	9.0–18.0	10.7–13.1
QCls31ubo-7A	RLT, RNL	IWA2896	7A	78.0	75.2	86.1	82.05	80.21	106.21	3.1–3.3	7.2–13.6	4.6–5.5
QCls32ubo-7A	RD, RLD, RSD, RSL, RTD, RTL, RSW, SRR, SMLER	IWB70728	7A	112.6	109.7	117.6	258.28	205.56	490.29	3.3–7.1	7.8–15.8	6.2–17.8
QCls33ubo-7A	RW, STN, RND	IWA2752	7A	130.5	127.4	140.7	564.25	550.57	621.01	3.0–4.4	7.7–15.7	4.4–11.0
QCls34ubo-7A	RDW, RMGR, RST	IWB61376	7A	203.4	200	206.4	721.40	717.99	724.49	3.1–4.0	7.5–9.8	4.8–7.3
QCls35ubo-7B	SALA, RTT	IWB36522	7B	0.0	0.0	6.5	3.35	0.43	6.14	3.8–4.2	8.2–10.3	9.1–11.2
QCls36ubo-7B	SALA, SALW, RDFP	IWB47779	7B	90.0	86.8	96.1	475.49	464.97	519.59	3.3–6.2	7.7–24.0	4.5–14.5

(Continues)

TABLE 3 (Continued)

QTL cluster (acronym)	Single component QTL (acronym)	Tag marker (SNP)	Chr. (no.)	QTL peak position (cM[a])	CI left (cM)	CI right (cM)	CI_peak (Mb[b])	CI left (Mb)	CI right (Mb)	-$\log_{10}(p)$ (range)	Effect range (%)	R^2 range (%)
QCls37ubo-7B	RLL, RLT	IWB54467	7B	114.2	111.6	120.4	583.84	574.08	593.69	3.2–3.8	9.6–11.2	7.3–8.2
QCls38ubo-7B	RND, SLT	IWB34900	7B	161.7	158.7	168.1	676.78	675.36	682.15	3.1–5.7	7.2–13.6	2.3–18.3
QCls39ubo-7B	RND, SLSW	IWB72833	7B	186.0	181.1	189.3	696.33	693.58	700.02	3.1–4.9	7.6–12.3	2.8–10.5

Note: RD, root depth (cm), whole root system; RD75, root depth, 75th percentile (cm), whole root system; RDFP, root deepening curve flex point (day), whole root system; RDW, root dry weight (g), whole root system; RLD, root dry weight (g), whole root system; RLL, root lateral length (cm), whole root system; RLT, density of nodal roots (cm/cm^2); RMDR, root maximum deepening rate (cm/day); RMGR, maximum root growth rate (cm/day); RND, root density in the deep layer, below 35 cm (cm·cm^2), nodal root system; RNL, root nodal length (cm), whole root system; RNS, root nodal-to-seminal ratio (cm/cm); RNT, density of nodal roots (cm/cm^2); RSD, root density in the deep layer, below 35 cm (cm·cm^2), seminal root system; RSL, root seminal length (cm), whole root system; RST, density of seminal roots (cm/cm^2); RSW, root seedling width; RTD, root density in the deep layer, below 35 cm (cm·cm^2), total root system; RTL, root total length (cm), total root system; RTT, density of total roots (cm/cm^2); RW, root system width (cm), total root system; SALA, shoot, average leaf area (cm^2); SALL, shoot, average leaf length (cm); SALW, shoot, average leaf width (cm); SLA, shoot, total leaf area (cm^2/leaf); SDW, shoot dry weight (g); SLN, shoot, leaf number per tiller (no.); SLSW, shoot, specific leaf weight (g/m^2); SLT, shoot, average leaf number per tiller (no.); SMLER, shoot, maximum leaf expansion rate (cm^2/day); SPAD, chlorophyll content; SRR, shoot-to-root ratio (g/g); STN, shoot, tiller number (no.).
Abbreviation: CI, confidence interval.
[a]As from the reference consensus genetic map for tetraploid wheat published in Maccaferri et al. (2015).
[b]As from the reference genome assembly of tetraploid wheat cultivar Svevo published in Maccaferri et al. (2019).

and nine shoot-trait-specific clusters (Table 3). No QTL showing a common effect to all three root types was found. In two cases, QTL for seminal and lateral roots shared the same CI (*QCls3.ubo-1B* and *QCls32.ubo-7A*). The large majority of QTL in clusters showed root class-specificity. No differences were observed in terms of preferential overlapping between root classes and shoot QTL, with QTL of the three root classes clustering with shoot QTL in five cases each (Figure 7). Three QTL clusters on chromosomes 1A (*QCls1.ubo-1A*), 1B (*QCls3.ubo-1B*), and 7A (*QCls32.ubo-7A*) showed extensive concomitant effects on 5, 10, and 9 traits, respectively (Table 3; Figures 5 and 6; Table S2).

Additionally, we projected platform-phenotyped wheat RSA QTL CIs found in two recent studies (Colombo et al., 2022; Ma et al., 2022) where authors screened BW and DW diversity panels at the adult plant stage in soil culture, using rhizo-tubes and pots, respectively (Figure 6).

3.6 | QTL clusters for plant vigor and/or deep rooting

Based on the increased impact of drought on cereal production worldwide due to climate change, deep rooting at the adult plant stage is one of the most interesting root traits. Five QTL clusters (*QCls1.ubo-1A, QCls3.ubo-1B, QCls8.ubo-2B, QCls25.ubo-6A*, and *QCls32.ubo-7A*) were particularly interesting based on their major effects on either proxy or adult stage traits.

QCls1.ubo-1A, a major QTL cluster localized at 75.1–84.5 cM on chr. Arm 1AL, affected maximum root depth (+15.8%), seminal and total roots below 35 cm (+17.3% and +13.1%), total root length (+11.8%), and root system width (+12.9%) with consistent direction of allelic effects.

A second major QTL cluster (*QCls3.ubo-1B*) for whole plant vigor, localized on chr. arm 1BL between 79.6 and 87.1 cM. *QCls3.ubo-1B*, affected 10 traits (Figure 8; Table S2 for details) showing concordant effects in all cases. *QCls3.ubo-1B* mainly affects deep rooting and the entire plant vigor with relative effects stronger in roots than shoots but not root system width. Therefore, it should be considered as a major QTL for root growth rate rather than a QTL for RGA. Interestingly, overlapping RSA QTL was found in the same region by Colombo et al. (2022) in two independent BW and DW panels (Figure 7a).

A QTL cluster for deep rooting (*QCls8.ubo-2B*) was identified on chr. arm 2BL specifically influencing maximum root deepening rate (−13.3%) and depth of root 75th percentile (+9.6%). A major QTL cluster for deep rooting was found on chr. arm 6AL (*QCls25.ubo-6A*), showing the strongest effect on root system width ($R^2 = 26.1\%$) and other root density distribution traits such as depth of the 75th percentile, maximum root density depth, seminal roots at the top of the rhizoboxes,

with opposite directional effect, as expected, and average leaf width and leaf area. As *QCls25.ubo-6A* impacted deep rooting mainly through RGA, it could be considered a QTL cluster rather specific for this trait.

Two additional QTL clusters for deep rooting were found on chromosome arm 7AL. The first (*QCls32.ubo-7A*) was a major QTL cluster involved in deep rooting, including nine QTLs in a 1.4-cM interval on chr. arm 7AL at position 109.7–117.6 cM. It is a major QTL cluster with significant effects on nine individual traits, including maximum root depth and total length of visible roots at depth (+15.7%, +14.9%), while showing contrasting effects for shoot-to-root dry biomass ratio (−12.9%), root-specific weight (−10.7%), and maximum leaf expansion rate (−7.8%). This cluster can therefore be considered as a major controller of shoot-to-root growth and biomass partitioning. A second cluster on chromosome 7A (*QCls33.ubo-7A*) was located on the 127.4- to 140.7-cM interval of the consensus map and showed specific effects for root system width and nodal root density in the deep layer, maximum root system width, nodal roots at depth, and TN. This QTL was also identified at the seedling stage in Maccaferri et al. (2016).

Most QTLs for deep rooting affected seminal root traits. In addition to deep-rooting QTL clusters, *QCls10.ubo-2B* showed a strong effect on root-to-shoot-biomass ratio with two prevailing alleles with contrasting effects on alleles favoring one or the other and affecting seminal root length and total root density below 35 cm.

A diagram of allelic effects for the main clusters and traits is depicted in Figure 5, while Table S3 reports detailed genotype ID, population structure ADMIXTURE Q membership coefficients, and best linear unbiased estimates (BLUEs) of phenotypic traits for the genotypes considered in rhizoboxes (this study) and in paper-screen evaluation (Canè et al., 2014). A major QTL cluster (*QCls15.ubo-3A*) affecting SDW, RSDW, lateral roots at depth, and leaf-specific weight was positioned on chromosome 3A at position 97.2–108.3 cM. Cluster *QCls30.ubo-7A* spanned a 11.7 cM wide c.i. (50.3–57.9 cM) and positively affected SDW, RSDW, root system width, nodal roots at depth, and nodal to seminal length ratio. Additionally, two major QTL clusters were located on chromosome arm 7AL (*QCls32.ubo-7A* and *QCls33.ubo-7A*), making the distal region of chromosome 7A a hot spot for root and shoot developmental QTL.

3.7 | QTL clusters specific for seminal, nodal, and lateral roots

Importantly, the rhizobox platform allowed us to discriminate between seminal, nodal, and lateral root trait apparatus, hence allowing us to identify QTL clusters with specific effects for each of the three root types. Few QTL/QTL clusters were specifically observed for seminal root only, whereas nodal and lateral roots showed a more specific genetic control. The development of the nodal (adventitious) roots is a component of the adult root apparatus also related to the plasticity of response to water and nutrient availability (C. Li et al., 2021). Contrary to seminal roots, nodal roots showed 10 QTLs with high specificity, including one singleton and six QTL clusters (*QCls2.ubo2-1B*, *QCls12.ubo-3A*, *QCls19.ubo-5A, QCls23.ubo-6A*, *QCls29.ubo-7A*, and *QCls30.ubo-7A*). However, these six QTL clusters were all highly specific for nodal root traits, except for *QCls29.ubo-7A*. Eighteen lateral roots QTLs/QTL clusters were identified, four as singletons and five as QTL cluster components, with one showing high specificity for lateral root traits (*QCls4.ubo-1B*). Interestingly, *QCls4.ubo-1B* can be classified as a major QTL with R^2 values of 16.3% for lateral root length and 19.8% for lateral root length (see Table S2).

As to the remaining QTL clusters, lateral root length QTL co-mapped with leaf area (opposite sign effect, one QTL) for the shoot traits and with total root length, root system width, total root length, and RSDW, always with a concordant sign effect (three QTLs), suggesting that most probably the determinants of these QTL clusters are loci involved in general root vigor, rather than loci specifically targeting lateral root emission. Conversely, the lateral root singletons are most probably encoded by loci with a more direct and exclusive lateral root-specific effect (per se effect).

3.8 | QTL clusters for shoot traits

While most of the QTL clusters for shoot traits showed effects on both shoot and root traits, nine QTL clusters only affected shoot traits. These included QTL clusters specific for (i) TN, leaf number, and leaves per tiller (*QCls6.ubo.2A*, *QCls16.ubo.3A*, *QCls33.ubo.7A*, and *QCls38.ubo.7B*) and (ii) leaf traits related to leaf area index, chlorophyll content, and photosynthetic capacity as *QCls17.ubo.4B*, *QCls*19.*ubo.5A*, *QCls*23.*ubo.5B*, and *QCls*29.*ubo.7A*. In particular, *QCls*29.*ubo.7A* had major effects for SPAD and leaf anatomy.

Among known phenology genes, *PPD-A1* CI did not overlap with any QTL, probably because plants were grown under long-day conditions. *PPD-B1* partially shared its CI with the QTL *QRtt.ubo-2B.2*, affecting total root length. *VRN-A1* was found to overlap with the QTL cluster *QCls21.ubo-5A* including two QTLs for total root length and leaf number. The other analyzed phenology genes, such as *VRN3(FT)* homologs did not overlap with any QTLs detected in this study.

Cluster	Tag_marker	Chr	Pos	Min_p.val
QCls1.ubo–1A	IWB35039	1	75.1	4.08
QCls2.ubo–1B	IWB59696	2	3.0	3.41
QCls3.ubo–1B	IWA7317	2	82.2	7.18
QCls4.ubo–1B	IWB72561	2	140.1	7.41
QCls5.ubo–2A	IWB54406	3	194.7	9.84
QCls6.ubo–2A	IWB9316	3	208.7	6.11
QCls7.ubo–2B	IWB28973	4	12.2	6.39
QCls8.ubo–2B	IWB22630	4	76.6	4.75
QCls9.ubo–2B	IWB66226	4	103.5	5.92
QCls10.ubo–2B	IWB22762	4	144.8	4.36
QCls11.ubo–2B	IWB19170	4	165.7	5.53
QCls12.ubo–2B	IWB28826	4	181.6	5.77
QCls13.ubo–3A	IWB44601	5	43.7	3.76
QCls14.ubo–3A	IWB48828	5	49.9	4.09
QCls15.ubo–3A	IWB58656	5	105.3	7.44
QCls16.ubo–3A	wPt–3133	5	123.5	4.41
QCls17.ubo–4B	IWB11925	8	34.4	6.13
QCls18.ubo–4B	IWB1109	8	83.1	3.78
QCls19.ubo–5A	IWB25728	9	14.3	10.82
QCls20.ubo–5A	IWB71919	9	67.3	3.35
QCls21.ubo–5A	IWA3887	9	146.5	4.06
QCls22.ubo–5A	IWA3335	9	199.6	8.02
QCls23.ubo–5B	IWB28778	10	47.4	9.73
QCls24.ubo–6A	IWB30925	11	62.1	7.04
QCls25.ubo–6A	IWB74235	11	122.1	10.07
QCls26.ubo–6B	IWB11783	12	74.9	6.05
QCls27.ubo–6B	IWB13090	12	90.1	4.54
QCls28.ubo–6B	IWB52925	12	154.6	4.18
QCls29.ubo–7A	IWB13845	13	14.1	11.82
QCls30.ubo–7A	IWB55999	13	53.1	4.88
QCls31.ubo–7A	IWA2896	13	78.0	3.29
QCls32.ubo–7A	IWB51612	13	112.6	7.08
QCls33.ubo–7A	IWA2752	13	130.5	4.43
QCls34.ubo–7A	IWB61376	13	203.4	4.04
QCls35.ubo–7B	IWB8973	14	0.0	4.15
QCls36.ubo–7B	IWB47779	14	90.0	6.19
QCls37.ubo–7B	IWB41721	14	114.2	3.78
QCls38.ubo–7B	IWB34900	14	161.7	5.67
QCls39.ubo–7B	IWB10818	14	186.0	4.90

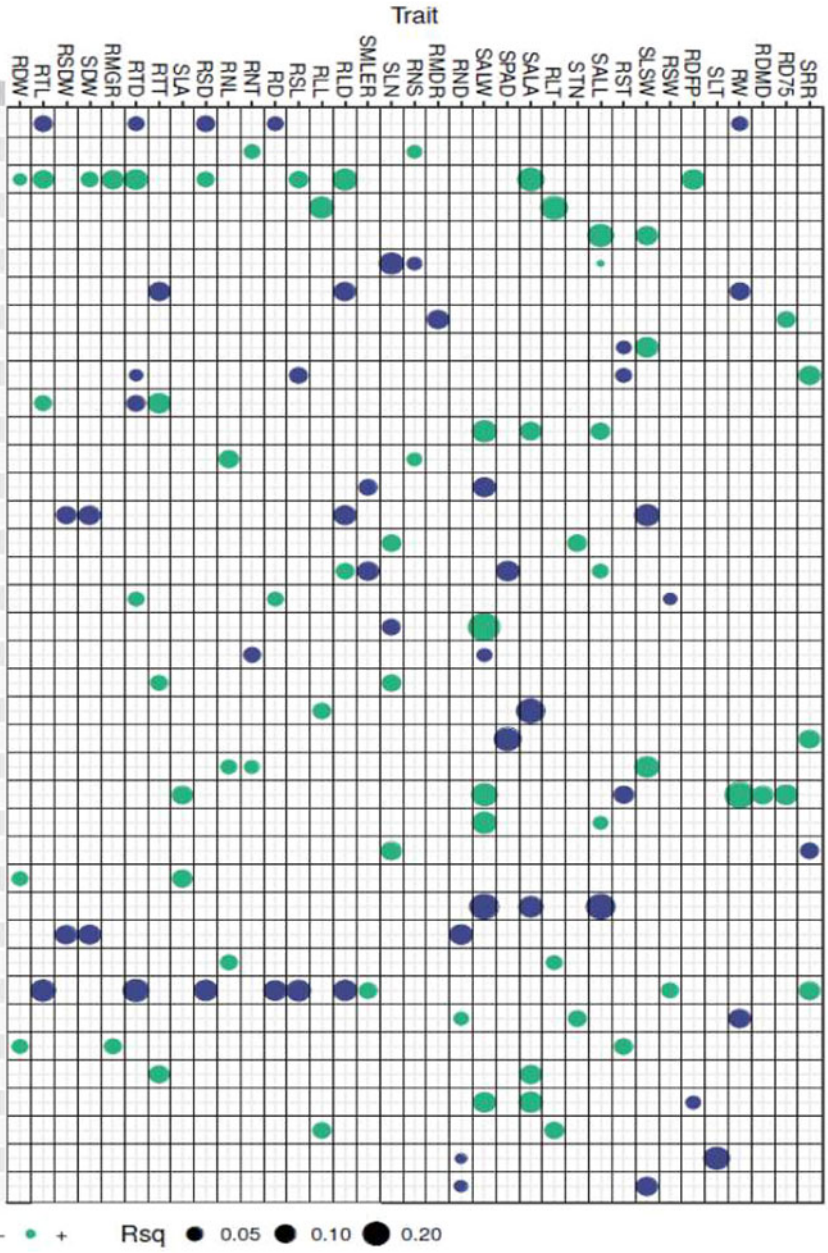

FIGURE 5 Summary results of the quantitative trait locus (QTL)-cluster analysis. R^2 and direction effect of the detected QTL clusters (more than two traits QTL in the same confidence interval). Cluster ID, tag marker, and its chromosome and position on the Maccaferri et al. (2015) consensus map, positions of the two most external significant markers of the QTL cluster, max –log10 (p).

3.9 | Haplotype analysis at the main QTL clusters suggests different selection strategies driven by different breeding environments

In this report, we present and analyze the haplotype effect and distribution of three prominent QTL clusters: *QCls3.ubo-1B*, which encompasses QTLs for a number of traits; *QCls25.ubo-6A*, with the most significant impact on root system width and RGA; and *QCls32.ubo-7A*, affecting both the shoot and root system with the strongest effect on shoot-to-root ratio. Haplotype analysis at these three major QTL clusters exhibited differential segregation patterns between the population structure groups, suggesting a role of these genomic regions in shaping RSA and its consequent response to breeding pressure.

At *QCls3.ubo-1B*, three haplotypes were detected in at least 5% of the population. Haplotypes *QCls3.ubo-1B*-2 and *QCls3.ubo-1B*-3 were genetically less distant than haplotype *QCls3.ubo-1B*-1 (Figure 8). The similarity between haplotypes 2 and 3 is confirmed by comparable and positive phenotypic effects suggesting the QTL causal mutation(s) predated the SNP mutations causing the divergence between

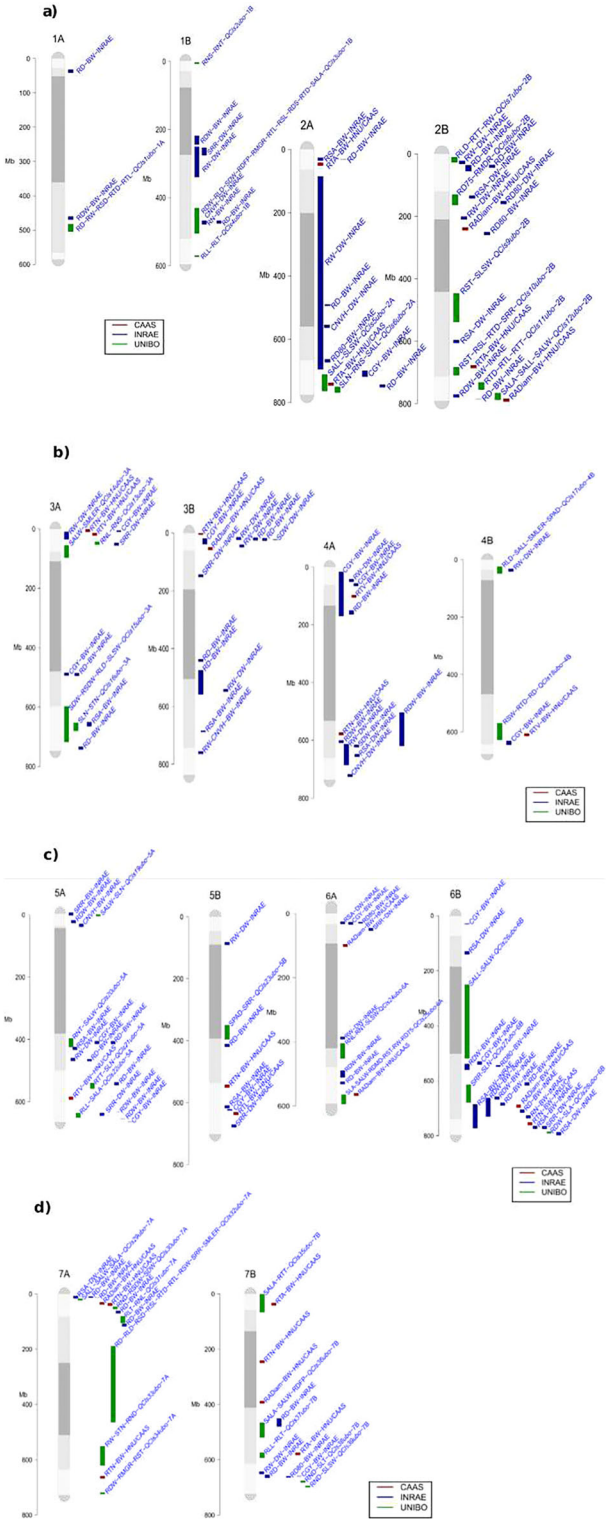

FIGURE 6 Root and shoot quantitative trait locus (QTL) clusters mapped on the physical map of Svevo durum wheat reference genome (Maccaferri et al., 2019). QTL confidence interval are reported for this study (green-bars, projected on chromosomes) and for root QTL identified by Ma et al. (2022) and Colombo et al. (2022), reported as red- and blue-bars, respectively. Chromosomes are partitioned in centromeric, pericentromeric, and distal regions using half-tone grays of increasing intensity, according to Maccaferri et al. (2019).

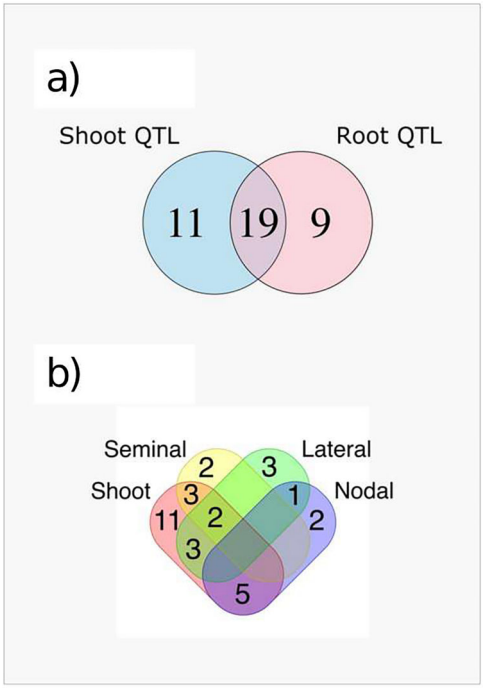

FIGURE 7 Venn's diagrams reporting the total quantitative trait locus (QTL) number and shared QTL number identified at different degrees of phenotype trait dissection for the shoot and root trait apparatus. (a) overlap between QTL for root and shoot traits, (b) overlap between the three main root types (namely, seminal, nodal and lateral roots) and shoot traits.

haplotypes 2 and 3. Haplotype 1 showed average phenotypic means lower than haplotypes 2 and 3 consistently across RDFP (root deepening curve flex point (day), whole root system), RDL, RMGR (maximum root growth rate [cm/day]), RTD (root density in the deep layer, below 35 cm [cm$\setminus$cm^2], total root system), and RSD (root density in the deep layer, below 35 cm [cm$\setminus$cm^2], seminal root system). As to haplotype distribution in the panel, *QCls3.ubo-1B*-1 prevailed in 91.3% of accessions of CIMMYT_80 subpopulation, while *QCls3.ubo-1B*-2 and *QCls3.ubo-1B*-3 prevailed in the other subpopulations.

At *QCls25.ubo-6A*, five haplotypes grouped into two clusters, the first including *QCls25.ubo-6A-2* and *QCls25.ubo-6A-5*, while the second included *QCls25.ubo-6A-1*, *QCls25.ubo-6A-3*, and *QCls25.ubo-6A-4*. Unlike *QCls3.ubo.1B*, haplotype effects did not reflect their phylogeny. *QCls25.ubo-6A-2* and *QCls25.ubo-6A-4* showed similar positive effects on root system width, maximum root density depth, depth of the 75th percentile, average leaf width, and leaf area, while showing negative effects on seminal roots. Haplotypes *QCls25.ubo-6A-1* and *QCls25.ubo-6A*-3 had opposite effects: they negatively affected root system width, average leaf width, and leaf area but positively affected seminal roots. Finally, the rare haplotype *QCls25.ubo-6A*-5 decreased root system width, while increasing seminal roots,

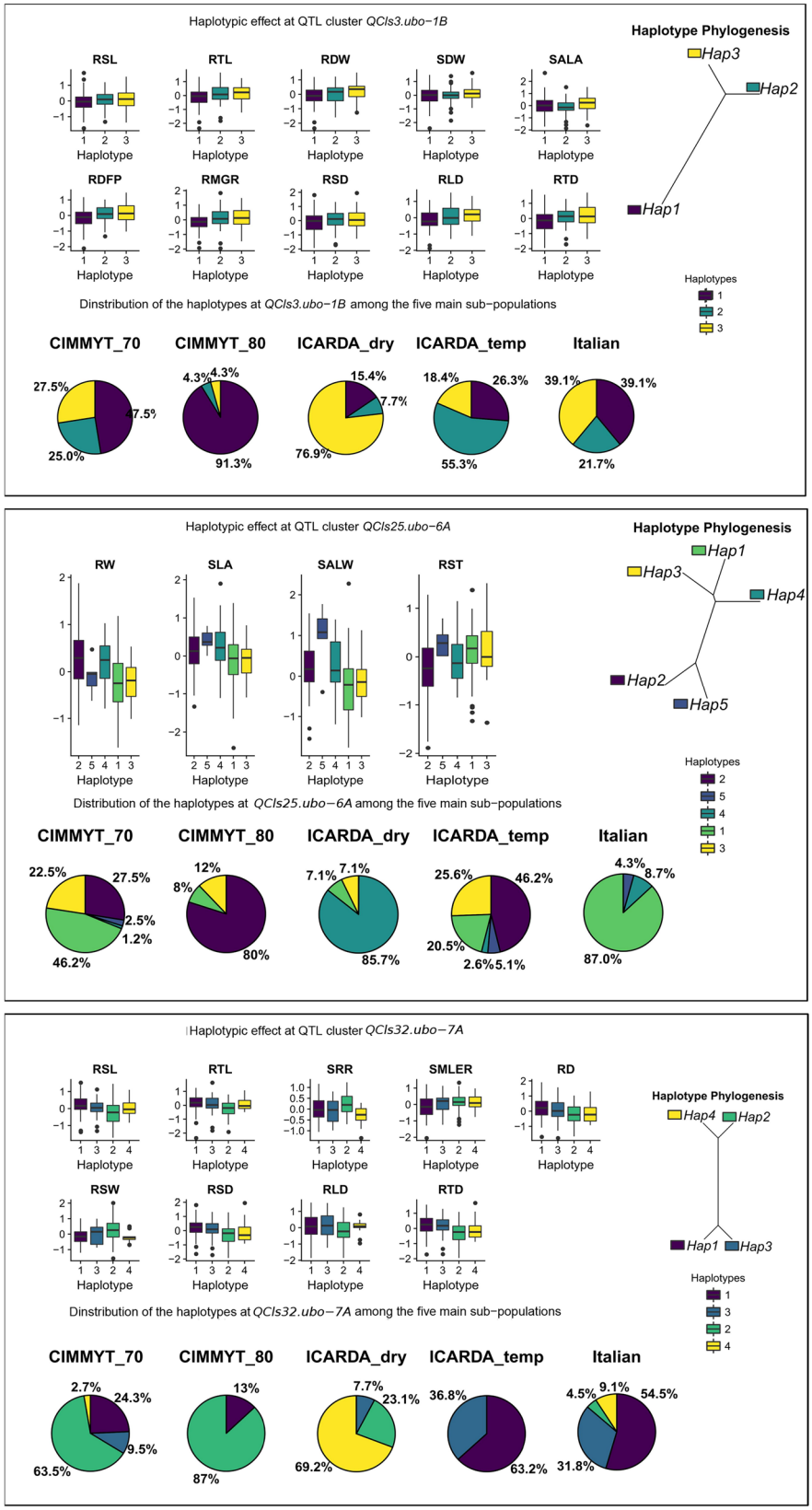

FIGURE 8 Quantitative trait locus (QTL) cluster haplotype distributions and effects for three main root system architecture (RSA) QTL clusters identified on chromosome 1B, 6A, and 7A.

average leaf width, and leaf area. As regards to haplotype distribution, the Italian subpopulation was largely dominated (87%) by the narrow-root system haplotype at *QCls25.ubo-6A*-1. The wide-root haplotypes *QCls25.ubo-6A*-4 and *QCls25.ubo-6A*-2 were predominant in ICARDA_dry and CIMMYT_80 (85.7% and 80%), respectively, while CIMMYT_70 subpopulation showed prevalence of the narrow-root *QCls25.ubo-6A-1* (46.2%) haplotype followed

by both *QCls25.ubo-6A-2* and *QCls25.ubo-6A-4* (both narrow-root haplotypes) and *QCls25.ubo-6A*-3 (22.5%).

Among the four main QTL clusters, *QCls32.ubo-7A* only was observed to include, in its CI, markers among the top 1% in terms of PC1, PC2, and PC3 loadings of population structure. The marker IWB57877 was the most predictive of population structure among the SNPs included in *QCls32.ubo-7A*. All markers of the corresponding haploblock, including IWB57877, were included in *QCls32.ubo-7A*. This haploblock showed four distinct and unrelated haplotypes. Summaries on the haplotypic effects are reported in Figure 8. *QCls32.ubo-7A* haplotype effects confirmed the significant marker-trait association identified by GWA. Haplotypes 1 and 3 showed the strongest effect on root deepening, positively affecting maximum root depth, seminal roots at depth, seminal root length, total roots at depth, and total root length while negatively affecting root-specific weight and maximum leaf expansion rate. Haplotypes 1 and 3 showed high genetic similarity and were largely prevalent in the *ICARDA_temp* and *Italian* subpopulations, where they were detected in 100% and 86.3% of the accessions. Haplotype 2, prevalent in the two *CIMMYT_70* and *CIMMYT_80* subpopulations, was associated to a more shoot-oriented carbon partitioning, favoring shoot-to-root ratio and maximum leaf expansion rate at the expense of root-deepening traits such as maximum root depth, lateral roots at depth, seminal roots at depth, seminal root length, total root at depth, and total root length. Haplotype 4, the rarest one, was largely represented in the *ICARDA_dry* subpopulation (69.2% of the accessions) and showed the strongest root-favorable carbon allocation, as well as the lowest root-specific weight of the four haplotypes. Nonetheless, this haplotype did not result in improved deep rooting.

Furthermore, deep rooting-related traits such as RW, RSL (root seminal length [cm], whole root system), and RTL (root total length [cm], total root system) were considered for the presence of genotypes with a concomitance of combined and consistent haplotype effects on the associated QTL clusters for each trait, as shown in Table 3 (Supporting Information Data 1). Based on the trait variability, positive or negative haplotype effects were determined for each QTL cluster at genotype level. The linear correlation between allelic effects and trait variability was low (R^2 between 3% and 18% for RW, 3% and 8% for RTL, and 3% and 10% for RSL), suggesting additional minor QTL and/or epistatic QTL–QTL interactions and unaccounted environmental effects concurred together. However, several examples of genotypes showing a cumulation of either positive or negative haplotype effects (multi-locus haplotypes) consistent with the corresponding phenotypic values can be observed. For example, for RW trait, four QTL clusters were associated with trait variability, namely, *QCls1ubo-1A*, *QCls7ubo-2B*, *QCls25ubo-6A*, and *QCls33ubo-7A*. Considering these QTL clusters in varieties at multi-locus level, Gallareta (= Altar_C84), Arcobaleno, Bolenga, CIMMYT 30th IDSN-23 (Bisu_1/Patka_3), CIMMYT 30th IDSN-52 (Kulrengi-Balikcil_8; Vanrikkse_6.2//1A-1D 2+12-5/3*WB881), Illora, INRA-1805 = Nassira, and Lahn showed a remarkable coincidence between cumulative haplotypes with positive effect at three-to-four RW QTLs and wide RW at phenotypic level. Interestingly, the above-mentioned cultivars with wide RW were mostly varieties of CIMMYT_80 origin/pedigree, related to Altar_C84 founder, known to be selected under bed-planting systems, and irrigation. Additionally, some old varieties directly related to some earlier Mediterranean landraces like Messapia, Trinakria, and Valbelice, also showed cumulative wide RW haplotypes and phenotypes. Consistently, genotypes that cumulated three-to-four QTL haplotypes estimated to have negative effects on RW in respect to the mean showed lower-than-average RW, as in the case of CIMMYT 30th IDSN-41 (DUKEM/3/RUFF/FGO//YAV79), CIMMYT 30th IDSN-266, Geromtel-1, Marsyr-1, and Moulsabil 2, mostly from the ICARDA breeding program, as expected.

As regards to RTL and RSL, two phenotypes correlated together and also related to efficient use of water, QTL clusters *QCls1ubo-1A*, *QCls3ubo-1B*, *QCls11ubo-2B*, and *QCls32ubo-7A* were considered for association to trait variation. Genotypes like Arcangelo, Gargano, Geromtel-1, and INRA-1808 = Amria, Tarek, ICA L 304-Lagonil-2, Lesina, Ofanto, and Telset-5 showed a concomitance and prevalence of positive haplotype effects associated to high RTL/RSL, and are all Italian and ICARDA genotypes adapted to drought conditions. Conversely, genotypes showing cumulative negative haplotype effects confirmed low RTL and RSL values and were identified as Aldeano, Aric_31708.70/3/Bo//C.de Chile/Br/4/Cit/Gta (ICARDA 78), Aus-1, Blk2, Borli, Chacan, Canyon, KRS/HAUCAN, Illora, INRA-1807 = Chaoui, INRA-1809 = Marouane, Ort-1, and Torrebianca (Supporting Information Data 1). These are a miscellanea of genotypes both of CIMMYT origin (Aldeano, Borli, Canyon, and Illora), consistent with the observation for RW as above, while several others are genotypes of mostly ICARDA origin, known to show a good resilience to drought and heat stress. In this case, we cannot rule out the possibility that their resilience to drought and heat is caused by physiological mechanisms other than deep rooting.

In summary, haplotype segregation patterns among and within subpopulations at the aforementioned QTL clusters exhibited a clear differentiation between the Italian and CIMMYT_80 materials. Notably, while the latter predominantly comprised haplotypes associated with diminished root system vigor (haplotype 1 at *QCls3.ubo-1B)*, wide root system development (haplotype 2 at *QCls25.ubo-6A*), and elevated shoot-to-root ratio (haplotype 2 at *QCls32.ubo-7A*), the Ital-

ian group was characterized by a pronounced prevalence of haplotypes that shaped RSA in a contrasting manner, that is, vigorous and narrow root system and low shoot-to-root ratio. The cumulative haplotype analysis for deep rooting traits reveals additive positive and negative effects for the multiple QTL clusters affecting RW, RSL, and RTL traits. Some examples of genotypes showing a remarkable prevalence of either positive or negative haplotype effects across all QTL clusters for each specific root trait correlated with extreme positive or negative RW, RSL, and RTL phenotypic values. In other cases, genotypes showing different and balanced combinations of QTL haplotypes with positive and negative effects at the selected QTL clusters were also observed, this time associated to variable trait expression. Although some genotypes showed a high consistency between cumulative haplotype effect and trait expression, others did not show a clear genotype–phenotype relationships suggesting that minor QTL effects, QTL interactions, or environmental variables influence the trait expression, thereby reducing the overall heritability and accuracy of QTL-based predictions.

3.10 | Candidate gene analysis and GO enrichment of the main QTL clusters

The genetic intervals of the main QTL clusters *QCls3.ubo-1B*, *QCls25.ubo-6A*, and *QCls32.ubo-7A* were explored for candidate gene analysis inspection. For each QTL cluster, the CI was obtained from Table 3 extracting all the genes included in the genomic region of *T. turgidum* 'Svevo' reference genome. A total number of 1910 genes among the three QTL clusters was obtained, namely, 594 for *QCls3.ubo-1B*, 368 for *QCls25.ubo-6A*, and 948 for *QCls32.ubo-7A*, together with information on gene description, GO information, gene orthologues in *A. thaliana*, *T. aestivum* 'Chinese Spring' RefSeq 1.1, *T. dicoccoides* 'Zavitan' v1.0 genomes, and paralogue genes on *T. turgidum* 'Svevo' genome (Table S4). In order to better describe the main gene categories of the QTL clusters, a GO enrichment analysis was performed obtaining information on the GO terms for MF, BP, and CC (Figure 9). As regards the GO:BP, the most significant GO enrichment ($p < 0.01$) included response to stress and defense response for *QCls25.ubo-6A*, and development of root/shoot and plant structure for *QCls32.ubo-7A*. With regard to *QCls3.ubo-1B*, GO enrichment categories (p-value < 0.05) were identified into the main categories of secondary metabolism, purine, and ATP biosynthesis process (Figure 9; Table S5).

The GO:MF enrichment ($p < 0.01$) highlighted oxidoreductase activity for *QCls3.ubo-1B* and chromatin binding and polysaccharide binding for *QCls25.ubo-6A*. Furthermore, MFs regarding secondary metabolism and biosynthesis activity, namely, protein transferase and ion binding activities, were enriched but with lower significance ($p < 0.05$) (Figure 9; Table S5). Finally, as regards GO CC (GO:BP) enrichment analysis, *QCls3.ubo-1B* and *QCls25.ubo-6A* showed significant associations (below <0.1) for CCs belonging to signaling pathways and protein arginilation. As to*QCls32.ubo-7A*, high significance ($p < 0.001$) was detected for root system development architecture (Figure 9; Table S5). To summarize, the GO enrichment analysis highlights BPs and MFs mainly involved in plant development, root development, metabolic activities, and biosynthesis processes.

In order to better discriminate candidate gene functions and networks, a restricted CI was identified by calculating ±2 Mb from the Tag SNP of QTLs *QCls3.ubo-1B*, *QCls25.ubo-6A*, and *QCls32.ubo-7A* (Table 3). The restricted CIs were explored for gene networks related to root development, morphology, and architecture by using Knetminer software, filtering for gene-to-gene network correspondence with $p < 0.05$ (Table S6). As regards *QCls3.ubo-1B*, the gene interval includes genes involved in root and lateral root morphology/development and embryonic differentiation, with a key phenotypic trait corresponding to gravitropism and root hair development (Table S6). The *QCls25.ubo-6A* gene network is highly significantly associated with root morphology, namely, root mass development, root meristem, root hair elongation, and lateral root morphogenesis. (Table S6). Finally, the genetic interval of *QCls32.ubo-7A* includes gene networks associated with root meristem and lateral root apical meristem (Table S6). The QTL clusters *QCls3.ubo-1B, QCls25.ubo-6A*, and *QCls32.ubo-7A* were explored also for transcriptomic expression on *T. aestivum* 'Chinese Spring' RefSeq 1.1, *A. thaliana*, and *O. sativa* subsp. *Japonica* (Supporting Information Data 2). As to *QCls3.ubo-1B*, the gene interval (from *TRITD1Bv1G158060* to *TRITD1Bv1G188240*) shows high expression values in roots in comparison to other tissues for *T. aestivum* orthologues, especially for *TRITD1Bv1G158720, TRITD1Bv1G160180, TRITD1Bv1G160350, TRITD1Bv1G162440*, and *TRITD1Bv1G163000* corresponding to ribosomal proteins, signaling proteins involved in gene transcription and cell differentiation. Similar results were identified also in *A. thaliana* orthologue expression atlas, where *TRITD1Bv1G158560* (MYB transcription factor), *TRITD1Bv1G159460* (Ataxin-3-like protein), *TRITD1Bv1G160180* (Adenine nucleotide alpha hydrolases-like superfamily protein), and *TRITD1Bv1G168260* (Abscisic acid receptor) showed a high expression in root tissues at the seedling stage and also in leaves at both the adult and seedling stages. On the other hand, as regards *O. sativa* sub japonica samples, higher expression in roots was detected for *TRITD1Bv1G165150* and *TRITD1Bv1G165190* corresponding to Aminotransferase-related family protein. As to *QCls25.ubo-6A*, the gene interval between *TRITD6Av1G216230* and *TRITD6Av1G227040*

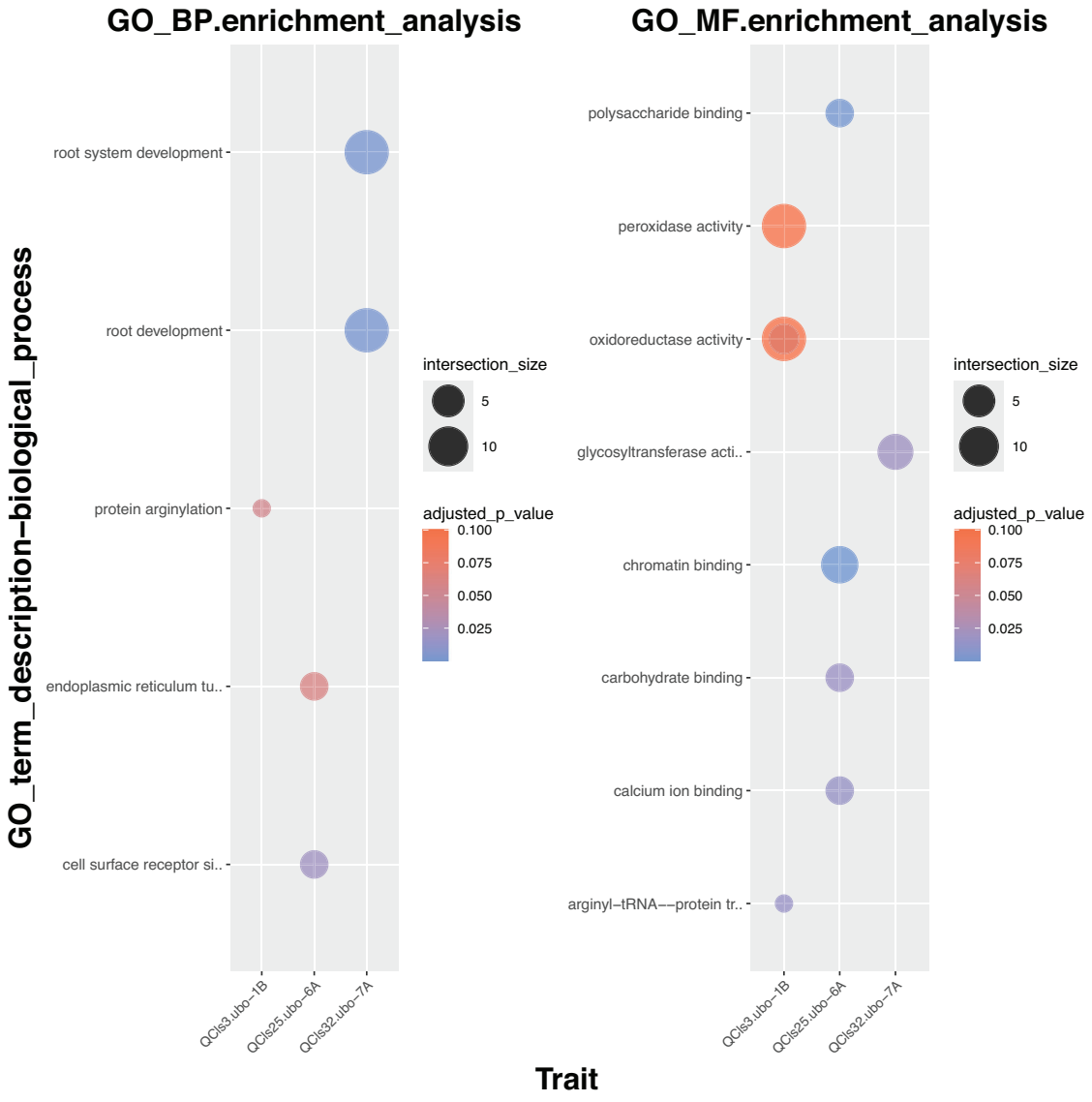

FIGURE 9 Gene onthology (GO) analysis on gene interval for three main quantitative trait locus (QTL) clusters *QCls3.ubo-1B*, *QCls25.ubo-6A*, and *QCls32.ubo-7A*. Genes were grouped for biological process (BP) and molecular functions (MF). Enriched functions were filtered for p-value < 0.1.

genes was explored. *T. aestivum* orthologue expression for *TRITD6Av1G219240* (O-methyltransferase) and *TRITD6Av1G223080* (Aquaporin) *showed* high expression in root tissues. In *A. thaliana* a high level of expression in root tissue was detected only for *TRITD6Av1G223140* (peptidyl-prolyl cis-trans isomerase) and *TRITD6Av1G218040* (germin-like protein 1-1) at the seedling stage. *Oryza sativa* subsp. japonica root tissue showed high expression in roots for *TRITD6Av1G218680* (nicotianamine synthase). As regards *QCls32.ubo-7A*, the gene network interval from *TRITD7Av1G085750* and *TRITD7Av1G180450* showed high gene expression in *T. aestivum* root tissue for *TRITD7Av1G176380* (Aquaporin) and *TRITD7Av1G176900* (Transcription activator BRG1 G). As regards *A. thaliana* root tissue, increased expression was detected for *TRITD7Av1G105030* (basic helix-loop-helix DNA-binding superfamily protein), *TRITD7Av1G133200* (polyadenylate-binding protein), *TRITD7Av1G160830* (60S acidic ribosomal protein P0), *TRITD7Av1G163420* (glyceraldehyde-3-phosphate dehydrogenase), *TRITD7Av1G165740* (calmodulin), *TRITD7Av1G174230* (CASP-like protein). *Oryza sativa* expression atlas showed increased gene expression for root at the seedling stage for *TRITD7Av1G171220* (glycolipid transfer protein domain-containing protein) and *TRITD7Av1G177730* (caffeic O-methyltransferase).

4 | DISCUSSION

4.1 | Root and shoot trait variation and related QTL clusters

For highly heritable traits with relatively simple genetic control, such as RGA, screening and selection of germplasm and segregating populations can be performed earlier at the seedling stage, thus allowing for quicker and higher throughput experiments (Sanguineti et al., 2007; El Hassouni et al., 2018). Conversely, other root traits such as adventitious and lateral root features, including final root density, root area, and specific root length, can be meaningfully assessed in adult plants only.

Once the biological and physiological relationships between the main trait and proxy traits are defined, whole-genome genotype data could be used to map on a unique framework multiple QTLs (QTLome, Salvi & Tuberosa, 2015) and QTL clusters for multiple traits (Solovieff et al., 2013; Mackay & Anholt, 2024). Therefore, knowledge on presence of QTLs and their alleles in crop germplasm has the potential for assisting breeders for a more informed choice of parents for mating (e.g., breeding by design, Peleman & Voort, 2003; genomics-assisted breeding, Sun et al., 2023).

In this study, we investigated both root and shoot traits. Although root dry weight and SDW traits showed high correlations, QTL clusters specific for root and shoot traits were also identified, highlighting the presence of genetic specificities, particularly at single root system component such as lateral and nodal (adventitious) roots (Freschet et al., 2021).

None of the detected QTL explained more than 30% of variance, which, in combination with h^2 values ranging from 0.31 to 0.77, confirms the quantitative nature of all traits herein considered. This is also confirmed by the limited overlap observed between the QTL CI reported in this study and the projected RSA QTL recently reported for independent BW and DW panels phenotyped at the adult plant stage in phenotyping platforms (Colombo et al., 2022; Ma et al., 2022).

Herein, despite a moderate correlation ($r = 0.33$*) was found between trait heritability and the variance explained by the QTL, the linearity between the h^2 and total QTL R^2 varied greatly among phenotypes, a well-known issue in GWAS, referred as "missing heritability" (Manolio et al., 2009). Remarkably, dissecting the complex traits into component traits of supposedly simpler genetic inheritance allowed us to enhance the dissection of the QTLome complexity and the accuracy of QTL discovery. Additionally, HTPP and RSA dissection for specific root traits on plants at advanced growth stages were made possible using HTPP and its imaging system, which is able to capture root system images at a frequency and resolution practically impossible to achieve with alternative phenotyping systems. Furthermore, we could dynamically investigate root classes development and their reciprocal relationships and effects on shoot growth.

From a breeding perspective, with the aim of maximizing selection efficiency and cost-effectiveness, it is highly relevant to prioritize traits and QTL as yield and stress adaptation proxies, particularly in view of their heritability (Tuberosa, 2012). As expected, at least for major QTL/QTL clusters, it is possible to identify to a certain degree the correspondence between RSA measured at the seedling stage with paper-roll or blue paper pouches and/or acrylic sheets and RSA traits observed at the late tillering stage in rhizoboxes (Canè et al., 2014; Maccaferri et al., 2016; Sanguineti et al., 2007) and, in the case of RGA, also in the field (Maccaferri et al., 2016), indicating that for some traits, cheaper and quicker phenotyping techniques might be suitable for breeding (Richard et al., 2015). *QCls3.ubo-1B* on chr. 1B at 79.6-87.1 cM, is one of the most notable QTL clusters reported also by Maccaferri et al. (2016). In this earlier study conducted in paper-roll and paper-screen, the 1B QTL cluster affected several below- and above-ground traits, including total root number, average root length, primary root length, and 1000-kernel weight in field experiments (Maccaferri et al., 2011). The role of this region in the control of root architecture has been confirmed in a durum × emmer biparental population (Iannucci et al., 2017). Interestingly, a study conducted on hexaploid wheat found the syntenic region of *QCls3.ubo-1B* to affect root dry weight (Y. Guo et al., 2012), and recently, the QTL was also identified by Colombo et al. (2022) and Ma et al. (2022). It would be, therefore, valuable to pursue *QCls3.ubo-1B* characterization in future studies and eventually its cloning.

QCls7.ubo-2BL (chromosome 2B, position 12.2–17.7 cM) affected total root length in the top 35 cm, lateral roots at depth, and root system width. Other experiments conducted on BW (Atkinson et al., 2015; Cao et al., 2014; Hamada et al., 2012; Ren et al., 2012), and DW (Maccaferri et al., 2016) confirm the involvement of this region in the control of root growth.

In the distal region of the long arm of chromosome 2B, we identified *QCls10.ubo-2B*, a major QTL cluster for total root length, total root length at depth, and total root length in the first 35 cm, which colocalized with major QTL for average root length, primary root length, and total root length found in paper-screen (Maccaferri et al., 2016).

Notably, *QCls25.ubo-6A* with the highest R^2 for RGA in paper-screen, mapped on chr. 6A with a QTL peak at 122.1 cM = 600.48 Mb, corresponded to the QTL with the highest R^2 (22%) for root system width in the rhizobox experiment, confirmed also by concomitant significant effects on RDMD, RST (density of seminal roots [cm/cm^2]), and RD75. Notably, the 6A QTL also showed a significant effect on active osmotic adjustment in controlled drought-stressed field trials carried out with the same DW panel herein considered (Condorelli et al., 2022). Interestingly, the 6A RGA QTL effect was never

identified in BW, neither at the seedling stage nor at adult plant, making this QTL a valuable case study for marker-assisted introgression in the BW germplasm toward ridging the genomic information and leveraging the valuable alleles of DW and BW gene pools (Maccaferri et al., 2015; Mazzucotelli et al., 2024). This QTL cluster aligned precisely with the corresponding RGA QTL found on the same durum materials characterized for RGA at seedling (Maccaferri et al., 2016). Additionally, the same QTL was identified in a durum elite nested association mapping population (Alahmad et al., 2019; Kang et al., 2024) and in an Ethiopian DW collection (Alemu et al., 2021). Interestingly, this very stable and robust RGA QTL is specific to tetraploid wheat, as it has not been reported yet in any QTL study targeted to seedling and/or adult RSA in BW. Thus, the effect of this major QTL deserves a more careful characterization, both with regard to its genetic control and direct exploitation in breeding for deep rooting.

An interesting QTL is *QCls32.ubo-7A*, the QTL cluster with significant effects on the highest number of investigated traits (nine). Located in the peri-centromeric region of chr. 7A, *QCls32.ubo-7A* affected most of the deep-rooting traits (Figure 7) and, importantly, also affected shoot-to-root ratio, an important trait in determining plant adaptation capability. Notably, Maccaferri et al. (2016), using the same association panel, showed that the same region was associated to a putative QTL for primary root length only; furthermore, the same authors report a QTL cluster in the same region for primary root volume and diameter and total root surface on a biparental RIL.

In the last decade, QTL studies have focused on seminal roots, observed at an early growth stage, for phenotyping capacity constraints (Christopher et al., 2013; Atkinson et al., 2015; Alemu et al., 2021). Only recently, the small grain cereal scientific community started to carry out genetic studies at more advanced growth stages, thus allowing them to better characterize more complex root trait phenotypes, such as root branching and lateral root emission (Beyer et al., 2018; L. Li et al., 2019). As an example, Howell et al. (2014) showed that a wheat/rye polymorphism on chromosome 1B/1R substitution region influenced seminal root length that was associated with a developmentally regulated arrest of the root apical meristem at a relatively late developmental stage. This is an example of how precise phenotyping is key to better characterizing nontrivial QTL effects.

In this study, similarly to Howell et al. (2014) and Colombo et al. (2022), phenotyping with the GROWSCREEN-Rhizo platform allowed us to characterize nontrivial phenotypes such as deep rooting and the relative ratio among seminal, nodal, and lateral roots in a wide range of genotypes, suitable for GWA analysis.

Recently, in view of their relevance for water and nutrient uptake, the role of nodal and, particularly lateral roots is being increasingly characterized by using advanced physiological, genetical, and genomics tools in *Arabidopsis* and in crops (Yu et al., 2016; Müller et al., 2024; Gonin et al., 2019; H. Guo et al., 2021; Tuberosa et al., 2021). The present study, particularly with the identification of major QTL clusters for deep rooting and lateral roots, aims to contribute toward the advancement in this area.

4.2 | Haplotypes analysis for the prioritized QTL clusters

Switching from simple bi-allelic SNP analysis to multi-SNP and multi-allelic haplotypes allowed for more accurately defining the allelic effects of QTL clusters on RSA traits. Selection history was associated to divergence for root traits in the wheat association panel.

At the two main QTL clusters, *QCls25.ubo-6A* and *QCls32.ubo-7A*, in both cases CIMMYT_80 varieties carried haplotypes conferring reduced root depth and/or vigor. Conversely, in the Italian subgroup, haplotypes for deep rooting and root-oriented carbon partitioning prevailed. Coincidence between selection history/geography and root traits was observed in a wheat association panel. Interestingly, haplotype frequency seems to reflect the strategy used in the main breeding programs. Haplotypes 1 and 3, associated with the deep-rooting phenotype, prevailed in Italian and *ICARDA_temp* subpopulations. Conversely to CIMMYT-derived lines, those belonging to the two above-mentioned groups were selected under rainfed Mediterranean conditions, where the deep-rooting phenotype allows for a better deep-water uptake. Notably, CIMMYT breeding programs have been traditionally conducted using artificial irrigation; in such conditions, haplotype 2, prevalent in CIMMYT subpopulations, could be beneficial due to a more shoot-oriented carbon partitioning and, finally, better agronomical performance. Accordingly, deep-rooting phenotypes could be useless, if not deleterious, in those conditions where water and nutrients are mainly present in the soil top layers as usually occurs under irrigation. Nevertheless, the evaluation of the effects of these QTL clusters on grain yield in a multi-environmental experimental setup remains challenging, particularly in an association mapping population due to the concomitant effects of other QTLs contributing to yield formation. Furthermore, a combined haplotype analysis was performed among QTL clusters shared by deep-rooting phenotypes such as RW, RTL, and RSL. Even if there is not a consistent correlation between trait variability and additive selected QTL clusters, it can be concluded that, in several cases, QTL clusters have all positive (or negative) effects for the related traits and have a strong positive (or negative) phenotypic value. Characterization of larger panels such as the Global Durum Panel (Mazzucotelli, Sciara et al., 2020) could provide further insights into the origin and spread of the most

promising haplotypes. In this perspective, further characterization is needed also for candidate gene analysis, exploiting larger panels to increase the recombination rate, refining the QTLs CIs, and screening favorable haplotypes genotypes with key molecular markers (such as KASP assays) tagging informative QTL clusters. However, the GO analysis, RNASeq database exploration, and gene network analysis showed interesting candidate genes and cellular pathways involved in root development, transcription factors and cellular signalling pathways, and root morphology traits. Namely, some of these MFs and gene categories overlapped with already known genes identified in previous root experiments, such as F-box domains of transcription factors, peroxidase, glycosyltransferases, peroxidases, and transporter proteins (Soriano & Alvaro, 2019). However, ad hoc transcriptomics and gene editing experiments with proper germplasm material need to be carried out to understand the key root trait regulators using larger germplasm resources.

5 | CONCLUSIONS

The GROWSCREEN-Rhizo platform allowed for an accurate and unprecedented genetic dissection of the QTLome governing the variability of root and shoot traits in DW. Additionally, HTP phenotyping allowed us to concomitantly investigate the development of seminal, nodal, and lateral roots up to the seventh leaf stage in adult plants. Genome-wide association analysis identified 39 QTL clusters for deep rooting and traits specific to the nodal and lateral roots, hence contributing to expand our knowledge on the genetic control of important root traits directly involved in water and nutrient uptake. Comparison with previous experiments based on different phenotyping protocols highlighted several QTLs consistently identified using different methodologies and genetic backgrounds, hence providing desirable targets for marker-assisted selection aimed at tailoring RSA.

The analysis of haplotype frequency at three QTL clusters suggested their putative role in DW breeding as related to the prevailing conditions targeted by breeding programs as to soil moisture availability and/or agronomic management. The most interesting haplotypes are being tested in biparental genetic backgrounds to more accurately define the environmental and management conditions able to optimize yield and yield stability. Notably, the haplotype frequency of two chromosome 6A and 7A clusters was significantly associated with root system depth, root specific weight and shoot/root ratio. Haplotype frequency analysis in different breeding lineages at chromosome 7A revealed a strong and contrasting selection pattern between the rainfed and the irrigated breeding programs conducted at ICARDA and CIMMYT, respectively, suggesting an indirect but important role of RSA features on grain yield in DW breeding and environmental adaptation.

Advances in genomics will allow us to more precisely identify the genetic determinants of complex traits governing crop resilience to stresses, and more efficiently exploit beneficial alleles through marker- and haplotype-based selection, also across gene pools, as in the case of durum and BW. More detailed approaches, including plant modeling, transcriptome and metabolome characterization, and carbohydrates homeostasis, will allow us to better understand the physiological mechanisms underlying important drought-adaptive traits.

AUTHOR CONTRIBUTIONS

Giuseppe Sciara: Conceptualization; data curation; methodology; software; visualization; writing—original draft; writing—review and editing. **Matteo Bozzoli**: Data curation; investigation; methodology; software; visualization; writing—review and editing. **Fabio Fiorani**: Conceptualization; investigation; methodology; supervision; writing—review and editing. **Kerstin A. Nagel**: Data curation; investigation; methodology; visualization; writing—review and editing. **Amina Ameer**: Data curation; software; visualization. **Silvio Salvi**: Conceptualization; investigation; project administration; resources; writing—review and editing. **Roberto Tuberosa**: Conceptualization; funding acquisition; investigation; project administration; resources; supervision; writing—review and editing. **Marco Maccaferri**: Conceptualization; data curation; formal analysis; investigation; project administration; supervision; validation; visualization; writing—original draft; writing—review and editing.

ACKNOWLEDGMENTS

This research was supported by the AGER project *From Seed to Pasta—Multidisciplinary approaches for a more sustainable and high-quality durum wheat production*, *Rooty—A root ideotype toolbox to support improved wheat yields* funded by the IWYP Consortium (project IWYP122), the EU project FP7-244374 (DROPS). Experiments were conducted at the IBG-2; Plant Science Institute, Forschungszentrum Jülich funded by the Program Oriented Funding of the Helmholtz Association.

CONFLICT OF INTEREST STATEMENT

The authors declare no conflicts of interest.

DATA AVAILABILITY STATEMENT

SNP Illumina Infinium *iSelect* wheat SNP array genotypic data of the UNIBO Durum Panel cultivars and breeding lines are publicly available in GrainGenes database at the Global Durum Genomic Resources page, available at https://wheat.pw.usda.gov/GG3/global_durum_genomic_resources as part of the Global Tetraploid Global Collection (TGC) and Global Durum Panel (GDP) resources.

Population structure ADMIXTURE Q membership coefficients, and best linear unbiased estimates (BLUES) phenotypic traits for the genotypes considered in rhizoboxes (this study) and in paper-screen evaluation (Canè et al., 2014) of the UNIBO Durum Panel cultivars and breeding lines are available in supporting information tables.

Single QTL genetic and physical position, including confidence interval, QTL peack, associated tag-SNP, and −log *p*-value of the associations are reported in supporting information tables.

The tetraploid consensus genetic map is available as part of supplementary materials of Maccaferri et al. (2015) at https://onlinelibrary.wiley.com/doi/abs/10.1111/pbi.12288.

The Svevo durum reference genome version 1 is available in NCBI at https://www.ncbi.nlm.nih.gov/datasets/genome/GCA_900231445.1/, and in GrainGenes at https://wheat.pw.usda.gov/jb/?data=/ggds/whe-svevo, and in EnsemblPlants at https://plants.ensembl.org/Triticum_turgidum/Info/Index

ORCID

Giuseppe Sciara https://orcid.org/0000-0001-9257-5490
Matteo Bozzoli https://orcid.org/0000-0002-4599-5334
Fabio Fiorani https://orcid.org/0000-0001-8775-1541
Kerstin A. Nagel https://orcid.org/0000-0003-3025-0388
Silvio Salvi https://orcid.org/0000-0002-0338-8894
Roberto Tuberosa https://orcid.org/0000-0001-9143-9569
Marco Maccaferri https://orcid.org/0000-0002-1935-3282

REFERENCES

Alahmad, S., El Hassouni, K., Bassi, F. M., Dinglasan, E., Youssef, C., Quarry, G., Aksoy, A., Mazzucotelli, E., Juhász, A., Able, J. A., Christopher, J., Voss-Fels, K. P., & Hickey, L. T. (2019). A major root architecture QTL responding to water limitation in durum eat. *Frontiers in Plant Science*, *10*, https://doi.org/10.3389/fpls.2019.00436

Alemu, A., Feyissa, T., Maccaferri, M., Sciara, G., Tuberosa, R., Ammar, K., Badebo, A., Acevedo, M., Letta, T., & Abeyo, B. (2021). Genome-wide association analysis unveils novel QTLs for seminal root system architecture traits in Ethiopian durum wheat. *BMC Genomics*, *22*(1), https://doi.org/10.1186/s12864-020-07320-4

Appels, R., Eversole, K., Stein, N., Feuillet, C., Keller, B., Rogers, J., Pozniak, C. J., Choulet, F., Distelfeld, A., Poland, J., Ronen, G., Sharpe, A. G., Barad, O., Baruch, K., Keeble-Gagnère, G., Mascher, M., Ben-Zvi, G., Josselin, A.-A., … Wang, L., The International Wheat Genome Sequencing Consortium (IWGSC). (2018). Shifting the limits in wheat research and breeding using a fully annotated reference genome. *Science*, *361*, eaar7191. https://doi.org/10.1126/science.aar7191

Atkinson, J. A., Pound, M. P., Bennett, M. J., & Wells, D. M. (2019). Uncovering the hidden half of plants using new advances in root phenotyping. *Current Opinion in Biotechnology*, *55*, 1–8. https://doi.org/10.1016/j.copbio.2018.06.002

Atkinson, J. A., Wingen, L. U., Griffiths, M., Pound, M. P., Gaju, O., Foulkes, M. J., Le Gouis, J., Griffiths, S., Bennett, M. J., King, J., & Wells, D. M. (2015). Phenotyping pipeline reveals major seedling root growth QTL in hexaploid wheat. *Journal of Experimental Botany*, *66*, 2283–2292. https://doi.org/10.1093/jxb/erv006

Atkinson, J. A., Wingen, L. U., Griffiths, M., Pound, M. P., Gaju, O., Foulkes, M. J., Le Gouis, J., Griffiths, S., Bennett, M. J., King, J., & Wells, D. M. (2015). Phenotyping pipeline reveals major seedling root growth QTL in hexaploid wheat. *Journal of Experimental Botany*, *66*(8), 2283–2292. https://doi.org/10.1093/jxb/erv006

Avni, R., Nave, M., Barad, O., Baruch, K., Twardziok, S. O., Gundlach, H., Hale, I., Mascher, M., Spannagl, M., Wiebe, K., Jordan, K. W., Golan, G., Deek, J., Ben-Zvi, B., Ben-Zvi, G., Himmelbach, A., Maclachlan, R. P., Sharpe, A. G., Fritz, A., … Distelfeld, A. (2017). Wild emmer genome architecture and diversity elucidate wheat evolution and domestication. *Science*, *357*, 93–97. https://doi.org/10.1126/science.aan0032

Barrett, J. C., Fry, B., Maller, J., & Daly, M. J. (2005). Haploview: Analysis and visualization of LD and haplotype maps. *Bioinformatics*, *21*, 263–265. https://doi.org/10.1093/bioinformatics/bth457

Basso, B., & Antle, J. (2020). Digital agriculture to design sustainable agricultural systems. *Nature Sustainability*, *3*, 254–256. https://doi.org/10.1038/s41893-020-0510-0

Bates, D., Mächler, M., Bolker, B., & Walker, S. (2015). Fitting linear mixed-effects models using lme4. *Journal of Statistical Software*, *67*, 1–48. https://doi.org/10.18637/jss.v067.i01

Beyer, S., Daba, S., Tyagi, P., Bockelman, H., Brown-Guedira, G., & Mohammadi, M. (2018). Loci and candidate genes controlling root traits in wheat seedlings—a wheat root GWAS. *Functional & Integrative Genomics*, *19*(1), 91–107. https://doi.org/10.1007/s10142-018-0630-z

Bhat, J. A., Yu, D., Bohra, A., Ganie, S. A., & Varshney, R. K. (2021). Features and applications of haplotypes in crop breeding. *Communications Biology*, *4*, Article 1266. https://doi.org/10.1038/s42003-021-02782-y

Bonferroni, C. E. (1936). Teoria statistica delle classi e calcolo delle probabilità. *Pubblicazioni del R Istituto Superiore di Scienze Economiche e Commerciali di Firenze*, *8*, 3–62.

Borrill, P., Ramirez-Gonzalez, R., & Uauy, C. (2016). expVIP: A customizable RNA-seq data analysis and visualization platform. *Plant Physiology*, *170*, 2172–2186. https://doi.org/10.1104/pp.15.01667

Bush, W. S., Chen, G., Torstenson, E. S., & Ritchie, M. D. (2009). LD-spline: Mapping SNPs on genotyping platforms to genomic regions using patterns of linkage disequilibrium. *BioData Mining*, *2*, Article 7. https://doi.org/10.1186/1756-0381-2-7

Canè, M. A., Maccaferri, M., Nazemi, G., Salvi, S., Francia, R., Colalongo, C., & Tuberosa, R. (2014). Association mapping for root architectural traits in durum wheat seedlings as related to agronomic performance. *Molecular Breeding*, *34*, 1629–1645. https://doi.org/10.1007/s11032-014-0177-1

Cao, P., Ren, Y., Zhang, K., Teng, W., Zhao, X., Dong, Z., Liu, X., Qin, H., Li, Z., Wang, D., & Tong, Y. (2014). Further genetic analysis of a major quantitative trait locus controlling root length and related traits in common wheat. *Molecular Breeding*, *33*, 975–985. https://doi.org/10.1007/s11032-013-0013-z

Chen, Y., Palta, J. A., Wu, P., & Siddique, K. H. M. (2019). Crop root systems and rhizosphere interactions. *Plant and Soil*, *439*, 1–5. https://doi.org/10.1007/s11104-019-04154-2

Choudhary, M., Wani, S. H., Kumar, P., Bagaria, P. K., Rakshit, S., Roorkiwal, M., & Varshney, R. K. (2019). QTLian breeding for climate resilience in cereals: Progress and prospects. *Functional and*

Integrative Genomics, *19*, 685–701. https://doi.org/10.1007/s10142-019-00684-1

Christopher, J., Christopher, M., Jennings, R., Jones, S., Fletcher, S., Borrell, A., Manschadi, A. M., Jordan, D., Mace, E., & Hammer, G. (2013). QTL for root angle and number in a population developed from bread wheats (*Triticum aestivum*) with contrasting adaptation to water-limited environments. *Theoretical and Applied Genetics*, *126*(6), 1563–1574. https://doi.org/10.1007/s00122-013-2074-0

Collins, N. C., Tardieu, F., & Tuberosa, R. (2008). Quantitative trait loci and crop performance under abiotic stress: Where do we stand? *Plant Physiology*, *147*, 469–486. https://doi.org/10.1104/pp.108.118117

Colombo, M., Roumet, P., Salon, C., Jeudy, C., Lamboeuf, M., Lafarge, S., Dumas, A. V., Dubreuil, P., Ngo, W., Derepas, B., Beauchêne, K., Allard, V., Le Gouis, J., & Rincent, R. (2022). Genetic analysis of platform-phenotyped root system architecture of bread and durum wheat in relation to agronomic traits. *Frontiers in Plant Science*, *13*, 853601. https://doi.org/10.3389/fpls.2022.853601

Condorelli, G. E., Newcomb, M., Groli, E. L., Maccaferri, M., Forestan, C., Babaeian, E., Tuller, M., White, J. W., Ward, R., Mockler, T., Shakoor, N., & Tuberosa, R. (2022). Genome wide association study uncovers the QTLome for osmotic adjustment and related drought adaptive traits in durum wheat. *Genes*, *13*, 293. https://doi.org.org/10.3390/genes13020293

Cooper, M., & Messina, C. D. (2021). Can we harness "enviromics" to accelerate crop improvement by integrating breeding and agronomy? *Frontiers in Plant Science*, *12*. https://doi.org/10.3389/fpls.2021.735143

Del Bianco, M., & Kepinski, S. (2018). Building a future with root architecture. *Journal of Experimental Botany*, *69*, 5319–5323. https://doi.org/10.1093/jxb/ery390

Diggle, A. J. (1988). ROOTMAP—A model in three-dimensional coordinates of the growth and structure of fibrous root systems. *Plant and Soil*, *105*, 169–178. https://doi.org.org/10.1007/BF02376780

Dyer, S. C., Austine-Orimoloye, O., Azov, A. G., Barba, M., Barnes, I., Barrera-Enriquez, V. P., Becker, A., Bennett, R., Beracochea, M., Berry, A., Bhai, J., Bhurji, S. K., Boddu, S., Branco Lins, P. R., Brooks, L., Ramaraju, S. B., Campbell, L. I., Martinez, M. C., Charkhchi, M., … Yates, A. D. (2024). Ensembl 2025. *Nucleic Acids Research*, *53*(D1), D948–D957. https://doi.org/10.1093/nar/gkae1071

El Hassouni, K., Alahmad, S., Belkadi, B., Filali-Maltouf, A., Hickey, L. T., & Bassi, F. M. (2018). Root system architecture and its association with yield under different water regimes in durum wheat. *Crop Science*, *58*, 2331–2346. https://doi.org/10.2135/cropsci2018.01.0076

Fleury, D., Jefferies, S., Kuchel, H., & Langridge, P. (2010). Genetic and genomic tools to improve drought tolerance in wheat. *Journal of Experimental Botany*, *61*, 3211–3222. https://doi.org/10.1093/jxb/erq152

Freschet, G. T., Pagès, L., Iversen, C. M., Comas, L. H., Rewald, B., Roumet, C., Klimešová, J., Zadworny, M., Poorter, H., Postma, J. A., Adams, T. S., Bagniewska-Zadworna, A., Bengough, A. G., Blancaflor, E. B., Brunner, I., Cornelissen, J. H. C., Garnier, E., Gessler, A., Hobbie, S. E., … Mccormack, M. L. (2021). A starting guide to root ecology: Strengthening ecological concepts and standardising root classification, sampling, processing and trait measurements. *New Phytologist*, *232*(3), 973–1122. https://doi.org.org/10.1111/nph.17572

Fusi, R., Rosignoli, S., Lou, H., Sangiorgi, G., Bovina, R., Pattem, J. K., Borkar, A. N., Lombardi, M., Forestan, C., Milner, S. G., Davis, J. L., Lale, A., Kirschner, G. K., Swarup, R., Tassinari, A., Pandey, B. K., York, L. M., Atkinson, B. S., Sturrock, C. J., … Salvi, S. (2022). Root angle is controlled by EGT1 in cereal crops employing an antigravitropic mechanism. *Proceedings of the National Academy of Sciences of the USA*, *119*, e2201350119. https://doi.org.org/10.1073/pnas.2201350119

Gioia, T., Nagel, K. A., Beleggia, R., Fragasso, M., Ficco, D. B. M., Pieruschka, R., De Vita, P., Fiorani, F., & Papa, R. (2015). Impact of domestication on the phenotypic architecture of durum wheat under contrasting nitrogen fertilization. *Journal of Experimental Botany*, *66*, 5519–5530. https://doi.org/10.1093/jxb/erv289

Gompertz, B. (1825). On the nature of the function expressive of the law of human mortality, and on a new mode of determining the value of life contingencies. *Philosophical Transactions of the Royal Society of London*, *115*, 513–583.

Gonin, M., Bergougnoux, V., Nguyen, T. D., Gantet, P., & Champion, A. (2019). What makes adventitious roots? *Plants*, *8*(7), 240. https://doi.org/10.3390/plants8070240

Guo, H., Ayalew, H., Seethepalli, A., Dhakal, K., Griffiths, M., Ma, X. F., & York, L. M. (2021). Functional phenomics and genetics of the root economics space in winter wheat using high-throughput phenotyping of respiration and architecture. *New Phytologist*, *232*, 98–112. https://doi.org/10.1111/nph.17329

Guo, J., Chen, G., Zhang, X., Li, T., Yu, H., & Liu, C. (2018). Quantitative trait locus analysis of adventitious and lateral root morphology of barley grown at low and high P. *Functional Plant Biology*, *45*, 957–967. https://doi.org/10.1071/FP17271

Guo, Y., Kong, F.-M., Xu, Y.-F., Zhao, Y., Liang, X., Wang, Y.-Y., An, D.-G., & Li, S.-S. (2012). QTL mapping for seedling traits in wheat grown under varying concentrations of N, P and K nutrients. *Theoretical and Applied Genetics*, *124*, 851–865. https://doi.org/10.1007/s00122-011-1749-7

Hamada, A., Nitta, M., Nasuda, S., Kato, K., Fujita, M., Matsunaka, H., & Okumoto, Y. (2012). Novel QTLs for growth angle of seminal roots in wheat (*Triticum aestivum* L.). *Plant and Soil*, *354*, 395–405. https://doi.org/10.1007/s11104-011-1075-5

Hassani-Pak, K., Singh, A., Brandizi, M., Hearnshaw, J., Parsons, J. D., Amberkar, S., Phillips, A. L., Doonan, J. H., & Rawlings, C. (2021). KnetMiner: A comprehensive approach for supporting evidence-based gene discovery and complex trait analysis across species. *Plant Biotechnology Journal*, *19*, 1670–1678. https://doi.org/10.1111/pbi.13583

Hawkesford, M. J. (2017). Genetic variation in traits for nitrogen use efficiency in wheat. *Journal of Experimental Botany*, *68*, 2627–2632. https://doi.org/10.1093/jxb/erx079

Hicks, S. C., Okrah, K., Paulson, J. N., Quackenbush, J., Irizarry, R. A., & Bravo, H. C. (2017). Smooth quantile normalization. *Biostatistics*, *19*, 185–198. https://doi.org/10.1093/biostatistics/kxx028

Howell, T., Moriconi, J. I., Zhao, X., Hegarty, J., Fahima, T., Santa-Maria, G. E., & Dubcovsky, J. (2018). A wheat/rye polymorphism affects seminal root length and is associated with drought and waterlogging tolerance. *Journal of Experimental Botany*, *70*, 4027–4037. https://doi.org/10.1093/jxb/erz169

Howell, T., Hale, I., Jankuloski, L., Bonafede, M., Gilbert, M., & Dubcovsky, J. (2014). Mapping a region within the 1RS.1BL translocation in common wheat affecting grain yield and canopy water status.

Theoretical and Applied Genetics, *127*(12), 2695–2709. https://doi.org/10.1007/s00122-014-2408-6

Iannucci, A., Marone, D., Russo, M. A., De Vita, P., Miullo, V., Ferragonio, P., Blanco, A., Gadaleta, A., & Mastrangelo, A. M. (2017). Mapping QTL for root and shoot morphological traits in a durum wheat × *T. dicoccum* segregating population at seedling stage. *International Journal of Genomics*, *2017*, 6876393. https://doi.org/10.1155/2017/6876393

Ito, K., Tanakamaru, K., Morita, S., Abe, J., & Inanaga, S. (2006). Lateral root development, including responses to soil drying, of maize (*Zea mays*) and wheat (*Triticum aestivum*) seminal roots. *Physiologia Plantarum*, *127*, 260–267. https://doi.org/10.1111/j.1399-3054.2006.00657.x

Jombart, T., Devillard, S., & Balloux, F. (2010). Discriminant analysis of principal components: A new method for the analysis of genetically structured populations. *BMC Genetics*, *11*, 94–95. https://doi.org/10.1186/1471-2156-11-94

Jombart, T. (2008). Adegenet: a R package for the multivariate analysis of genetic markers. *Bioinformatics*, *24*(11), 1403–1405. https://doi.org/10.1093/bioinformatics/btn129

Joshi, S., Chinnusamy, V., & Joshi, R. (2022). Root system architecture and omics approaches for belowground abiotic stress tolerance in plants. *Agriculture*, *12*, 1677. https://doi.org/10.3390/agriculture12101677

Kadam, N. N., Yin, X., Bindraban, P. S., Struik, P. C., & Jagadish, K. S. V. (2015). Does morphological and anatomical plasticity during the vegetative stage make wheat more tolerant of water deficit stress than rice? *Plant Physiology*, *167*, 1389–1401. https://doi.org/10.1104/pp.114.253328

Kang, Y., Rambla, C., Haeften, S. V., Fu, B., Akinlade, O., Potgieter, A. B., Borrell, A. K., Mace, E., Jordan, D. R., Alahmad, S., & Hickey, L. T. (2024). Seminal root angle is associated with root system architecture in durum wheat. *Food and Energy Security*, *13*, e570. https://doi.org/10.1002/fes3.570

Kemp, C. D. (1960). Methods of estimating the leaf area of grasses from linear measurements. *Annals of Botany*, *24*, 491–499. https://doi.org/10.1093/oxfordjournals.aob.a083723

Kenobi, K., Atkinson, J. A., Wells, D. M., Gaju, O., De Silva, J. G., Foulkes, M. J., Dryden, I. L., Wood, A. T. A., & Bennett, M. J. (2017). Linear discriminant analysis reveals differences in root architecture in wheat seedlings related to nitrogen uptake efficiency. *Journal of Experimental Botany*, *68*, 4969–4981. https://doi.org/10.1093/jxb/erx300

Kimura, M., & Crow, J. F. (1964). The number of alleles that can be maintained in a finite population. *Genetics*, *49*(4), 725–738. https://doi.org/10.1093/genetics/49.4.725

Kitomi, Y., Hanzawa, E., Kuya, N., Inoue, H., Hara, N., Kawai, S., Kanno, N., Endo, M., Sugimoto, K., Yamazaki, T., Sakamoto, S., Sentoku, N., Wu, J., Kanno, H., Mitsuda, N., Toriyama, K., Sato, T., & Uga, Y. (2020). Root angle modifications by the DRO1 homolog improve rice yields in saline paddy fields. *Proceedings of the National Academy of Sciences of the USA*, *117*, 21242–21250. https://doi.org/10.1073/pnas.2005911117

Koevoets, I. T., Venema, J. H., Elzenga, J. T. M., & Testerink, C. (2016). Roots withstanding their environment: Exploiting root system architecture responses to abiotic stress to improve crop tolerance. *Frontiers in Plant Science*, *31*, 1335. https://doi.org/10.3389/fpls.2016.01335

Langridge, P., Alaux, M., Almeida, N. F., Ammar, K., Baum, M., Bekkaoui, F., Bentley, A. R., Beres, B. L., Berger, B., Braun, H.-J., Brown-Guedira, G., Burt, C. J., Caccamo, M. J., Cattivelli, L., Charmet, G., Civáň, P., Cloutier, S., Cohan, J.-P., Devaux, P. J., … Zhang, X. (2022). Meeting the challenges facing wheat production: The strategic research agenda of the Global Wheat Initiative. *Agronomy*, *12*, 2767. https://doi.org/10.3390/agronomy12112767

Le Roux, M. S., Kunert, K. J., Cullis, C. A., & Botha, A. M. (2024). Unlocking wheat drought tolerance: The synergy of omics data and computational intelligence. *Food and Energy Security*, *13*, e70024. https://doi.org/10.1002/fes3.70024

Li, H., Liu, N., Shao, L., Liu, X., Sun, H., Chen, S., & Zhang, X. (2025). Changes in root growth and water uptake contribute to the yield and water productivity improvement in winter wheat during the past three decades: A case study in the North China Plain. *Agricultural Water Management*, *313*, 109482. https://doi.org/10.1016/j.agwat.2025.109482

Li, C., Li, L., Reynolds, M. P., Wang, J., Chang, X., Mao, X., & Jing, R. (2021). Recognizing the hidden half in wheat: root system attributes associated with drought tolerance. *Journal of Experimental Botany*, *72*(14), 5117–5133. https://doi.org/10.1093/jxb/erab124

Li, L., Peng, Z., Mao, X., Wang, J., Chang, X., Reynolds, M., & Jing, R. (2019). Genome-wide association study reveals genomic regions controlling root and shoot traits at late growth stages in wheat. *Annals of Botany*, *124*(6), 993–1006. https://doi.org/10.1093/aob/mcz041

Liang, X., Reham, S. U., Zhiqi, W., Raza, M. A., Haider, I., Khalid, M. H. B., Saeed, A., Iqbal, Z., Fatima, S., & Siddiqa, A. (2024). Impacts of conservation tillage on agricultural land development: A review. *Journal of Soil Science and Plant Nutrition*, *25*(1), 428–449.

Liu, H., Fiorani, F., Jäck, O., Colombi, T., Nagel, K. A., & Weih, M. (2021). Shoot and root traits underlying genotypic variation in early vigor and nutrient accumulation in spring wheat grown in high-latitude light conditions. *Plants*, *10*, 174. https://doi.org/10.3390/plants10010174

Lynch, J. P. (2013). Steep, cheap and deep: An ideotype to optimize water and N acquisition by maize root systems. *Annals of Botany*, *112*, 347–357. https://doi.org/10.1093/aob/mcs293

Lynch, J. P. (2022). Harnessing root architecture to address global challenges. *The Plant Journal*, *109*, 415–431. https://doi.org.org/10.1111/tpj.15560

Müller, B., Herrmann, M. N., Lewandowski, I., Müller, T., Hartung, J., & Bauerle, A. (2024). The effect of biobased N and P fertilizers in a winter wheat–ryegrass crop rotation. *Agronomy*, *14*(10), 2424. https://doi.org/10.3390/agronomy14102424

Müllner, D. (2013). fastcluster: Fast hierarchical, agglomerative clustering routines for R and Python. *Journal of Statistical Software*, *53*(9), https://doi.org/10.18637/jss.v053.i09

Ma, J., Zhao, D., Tang, X., Yuan, M., Zhang, D., Xu, M., Duan, Y., Ren, H., Zeng, Q., Wu, J., Han, D., Li, T., & Jiang, L. (2022). Genome-wide association study on root system architecture and identification of candidate genes in wheat (*Triticum aestivum* L.). *International Journal of Molecular Sciences*, *23*, 1843. https://doi.org/10.3390/ijms23031843

Maccaferri, M., Bruschi, M., & Tuberosa, R. (2022). Sequence-based marker assisted selection in wheat. In M. P. Reynolds & H.-J. Braun (Eds.), *Wheat improvement: Food security in a changing climate* (pp. 513–538). Springer International Publishing. https://doi.org/10.1007/978-3-030-90673-3

Maccaferri, M., El-Feki, W., Nazemi, G., Salvi, S., Canè, M. A., Colalongo, M. C., Stefanelli, S., & Tuberosa, R. (2016). Prioritizing quantitative trait loci for root system architecture in tetraploid wheat.

Journal of Experimental Botany, *67*, 1161–1178. https://doi.org/10.1093/jxb/erw039

Maccaferri, M., Harris, N. S., Twardziok, S. O., Pasam, R. K., Gundlach, H., Spannagl, M., Ormanbekova, D., Lux, T., Prade, V. M., Milner, S. G., Himmelbach, A., Mascher, M., Bagnaresi, P., Faccioli, P., Cozzi, P., Lauria, M., Lazzari, B., Stella, A., Manconi, A., … Cattivelli, L. (2019). Durum wheat genome highlights past domestication signatures and future improvement targets. *Nature Genetics*, *51*, 885–895. https://doi.org/10.1038/s41588-019-0381-3

Maccaferri, M., Ricci, A., Salvi, S., Milner, S. G., Noli, E., Martelli, P. L., Casadio, R., Akhunov, E., Scalabrin, S., Vendramin, V., Ammar, K., Blanco, A., Desiderio, F., Distelfeld, A., Dubcovsky, J., Fahima, T., Faris, J., Korol, A., Massi, A., … Tuberosa, R. (2015). A high-density, SNP-based consensus map of tetraploid wheat as a bridge to integrate durum and bread wheat genomics and breeding. *Plant Biotechnology Journal*, *13*, 648–663. https://doi.org/10.1111/pbi.12288

Maccaferri, M., Sanguineti, M. C., Demontis, A., El-Ahmed, A., Garcia Del Moral, L., Maalouf, F., Nachit, M., Nserallah, N., Ouabbou, H., Rhouma, S., Royo, C., Villegas, D., & Tuberosa, R. (2011). Association mapping in durum wheat grown across a broad range of water regimes. *Journal of Experimental Botany*, *62*, 409–438. https://doi.org/10.1093/jxb/erq287

Mackay, T. F., & Anholt, R. R. (2024). Pleiotropy, epistasis and the genetic architecture of quantitative traits. *Nature Reviews Genetics*, *25*, 639–657. https://doi.org/10.1038/s41576-024-00711-3

Manolio, T. A., Collins, F. S., Cox, N. J., Goldstein, D. B., Hindorff, L. A., Hunter, D. J., Mccarthy, M. I., Ramos, E. M., Cardon, L. R., Chakravarti, A., Cho, J. H., Guttmacher, A. E., Kong, A., Kruglyak, L., Mardis, E., Rotimi, C. N., Slatkin, M., Valle, D., Whittemore, A. S., … Visscher, P. M. (2009). Finding the missing heritability of complex diseases. *Nature*, *461*, 747–753. https://doi.org/10.1038/nature08494

Manschadi, A. M., Christopher, J., deVoil, P., & Hammer, G. L. (2006). The role of root architectural traits in adaptation of wheat to water-limited environments. *Functional Plant Biology*, *33*, 823–837. https://doi.org/10.1071/FP06055

Manschadi, A. M., Hammer, G. L., Christopher, J. T., & deVoil, P. (2008). Genotypic variation in seedling root architectural traits and implications for drought adaptation in wheat (*Triticum aestivum* L.). *Plant and Soil*, *303*, 115–129. https://doi.org/10.1007/s11104-007-9492-1

Manske, G. G. B., & Vlek, P. L. G. (2002). Root architecture—Wheat as a model plant. In Y. Waisel, A. Eshel, T. Beeckman, & U. Kafkafi (Eds.), *Plant roots: The hidden half* (pp. 249–260). Marcel Dekker Inc. https://doi.org/10.1201/9780203909423-24

Maqbool, S., Hassan, M. A., Xia, X., York, L. M., Rasheed, A., & He, Z. (2022). Root system architecture in cereals: Progress, challenges and perspective. *The Plant Journal*, *110*, 23–42. https://doi.org/10.1111/tpj.15669

Masle, J., & Passioura, J. B. (1987). The effect of soil strength on the growth of young wheat plants. *Australian Journal of Plant Physiology*, *14*, 643–656. https://doi.org/10.1071/PP9870643

Mazzucotelli, E., Mastrangelo, A. M., Desiderio, F., Barabaschi, D., Maccaferri, M., Tuberosa, R., & Cattivelli, L. (2024). Gene flow between tetraploid and hexaploid wheat for breeding innovation. In R. Appels, K. Eversole, C. Feuillet, & D. Gallagher (Eds.), *The wheat genome* (pp. 135–163). Springer.

Mazzucotelli, E., Sciara, G., Mastrangelo, A. M., Desiderio, F., Xu, S. S., Faris, J., Hayden, M. J., Tricker, P. J., Ozkan, H., Echenique, V., Steffenson, B. J., Knox, R., Niane, A. A., Udupa, S. M., Longin, F. C. H., Marone, D., Petruzzino, G., Corneti, S., Ormanbekova, D., … Bassi, F. M. (2020). The global durum wheat panel (GDP): An international platform to identify and exchange beneficial alleles. *Frontiers in Plant Science*, *11*, 569905. https://doi.org/10.3389/fpls.2020.569905

Moreno, P., Fexova, S., George, N., Manning, J. R., Miao, Z., Mohammed, S., Muñoz-Pomer, A., Fullgrabe, A., Bi, Y., Bush, N., Iqbal, H., Kumbham, U., Solovyev, A., Zhao, L., Prakash, A., García-Seisdedos, D., Kundu, D. J., Wang, S., Walzer, M., … Papatheodorou, I. (2022). Expression Atlas update: Gene and protein expression in multiple species. *Nucleic Acids Research*, *50*, D129–D140. https://doi.org/10.1093/nar/gkab1030

Nagel, K. A., Putz, A., Gilmer, F., Heinz, K., Fischbach, A., Pfeifer, J., Faget, M., Blossfeld, S., Ernst, M., Dimaki, C., Kastenholz, B., Kleinert, A.-K., Galinski, A., Scharr, H., Fiorani, F., & Schurr, U. (2012). GROWSCREEN-Rhizo is a novel phenotyping robot enabling simultaneous measurements of root and shoot growth for plants grown in soil-filled rhizoboxes. *Functional Plant Biology*, *39*, 891–904. https://doi.org/10.1071/FP12023

Nakhforoosh, A., Nagel, K. A., Fiorani, F., & Bodner, G. (2021). Deep soil exploration vs. topsoil exploitation: Distinctive rooting strategies between wheat landraces and wild relatives. *Plant and Soil*, *459*, 397–421. https://doi.org/10.1007/s11104-020-04794-9

Nehe, A. S., Foulkes, M. J., Ozturk, I., Rasheed, A., York, L., Kefauver, S. C., Ozdemir, F., & Morgounov, A. (2021). Root and canopy traits and adaptability genes explain drought tolerance responses in winter wheat. *PLoS One*, *16*, e0242472. https://doi.org/10.1371/journal.pone.0242472

Nouraei, S., Mia, M. S., Liu, H., Turner, N. C., & Yan, G. (2024). Genome-wide association study of drought tolerance in wheat (*Triticum aestivum* L.) identifies SNP markers and candidate genes. *Molecular Genetics and Genomics*, *299*(1). https://doi.org/10.1007/s00438-024-02104-x

Ober, E. S., Alahmad, S., Cockram, J., Forestan, C., Hickey, L. T., Kant, J., Maccaferri, M., Marr, E., Milner, M., Pinto, F., Rambla, C., Reynolds, M., Salvi, S., Sciara, G., Snowdon, R. J., Thomelin, P., Tuberosa, R., Uauy, C., Voss-Fels, K. P., … Watt, M. (2021). Wheat root systems as a breeding target for climate resilience. *Theoretical and Applied Genetics*, *134*(6), 1645–1662. https://doi.org/10.1007/s00122-021-03819-w

Odone, A., Changdar, S., & Thorup-Kristensen, K. (2025). Winter wheat phenotyping for deep root growth and function, reduced water stress and increased uptake of deep N and water. *Annals of Botany*, https://doi.org.10.1093/aob/mcaf160

Odone, A., & Thorup-Kristensen, K. (2025). Modern wheat has deeper roots than ancient wheats: is this an adaptation to higher productivity? *Annals of Botany*, https://doi.org/10.1093/aob/mcaf065

Olatunji, D., Geelen, D., & Verstraeten, I. (2017). Control of endogenous auxin levels in plant root development. *International Journal in Molecular Sciences*, *18*, 2587. https://doi.org/10.3390/ijms18122587

Olivares-Villegas, J. J., Reynolds, M. P., & McDonald, G. K. (2007). Drought-adaptive attributes in the Seri/Babax hexaploid wheat population. *Functional Plant Biology*, *34*(3), 189–203. https://doi.org/10.1071/fp06148

Palta, J. A., Chen, X., Milroy, S. P., Rebetzke, G. J., Dreccer, M. F., & Watt, M. (2011). Large root systems: Are they useful in adapting wheat to dry environments? *Functional Plant Biology*, *38*, 347–354. https://doi.org/10.1071/FP11031

Paradis, E., & Schliep, K. (2018). ape 5.0: An environment for modern phylogenetics and evolutionary analyses in R. *Bioinformatics*, *35*, 526–528. https://doi.org/10.1093/bioinformatics/bty633

Parasurama, S., Banan, D., Yun, K., Doty, S., & Kim, S. H. (2023). Bridging time-series image phenotyping and functional–structural plant modeling to predict adventitious root system architecture. *Plant Phenomics*, *5*, 0127. https://doi.org/10.34133/plantphenomics.0127

Passot, S., Moreno-Ortega, B., Moukouanga, D., Balsera, C., Guyomarc'h, S., Lucas, M., Lobet, G., Laplaze, L., Muller, B., & Guédon, Y. (2018). A new phenotyping pipeline reveals three types of lateral roots and a random branching pattern in two cereals. *Plant Physiology*, *177*, 896–910. https://doi.org/10.1104/pp.17.01648

Peleman, J. D., & Van Der Voort, J. R. (2003). Breeding by design. *Trends in Plant Science*, *8*, 330–334. https://doi.org/10.1016/S1360-1385(03)00134-1

Peng, B., Liu, X., Dong, X., Xue, Q., Neely, C. B., Marek, T., Ibrahim, A. M. H., Zhang, G., Leskovar, D. I., & Rudd, J. C. (2019). Root morphological traits of winter wheat under contrasting environments. *Journal of Agronomy and Crop Science*, *205*(6), 571–585. https://doi.org/10.1111/jac.12360

Poorter, H., Hummel, G. M., Nagel, K. A., Fiorani, F., Von Gillhaussen, P., Virnich, O., Schurr, U., Postma, J. A., Van De Zedde, R., & Wiese-Klinkenberg, A. (2023). Pitfalls and potential of high-throughput plant phenotyping platforms. *Frontiers in Plant Science*, *14*, 1233794. https://doi.org.org/10.3389/fpls.2023.1233794

Pritchard, J. K., Stephens, M., & Donnelly, P. (2000). Inference of population structure using multilocus genotype data. *Genetics*, *155*(2), 945–959. https://doi.org/10.1093/genetics/155.2.945

Rafalski, J. A. (2002). Novel genetic mapping tools in plants: SNPs and LD-based approaches. *Plant Science*, *162*, 329–333. https://doi.org.org/10.1016/S0168-9452(01)00587-8

Ramírez-González, R. H., Borrill, P., Lang, D., Harrington, S. A., Brinton, J., Venturini, L., Davey, M., Jacobs, J., Van Ex, F., Pasha, A., Khedikar, Y., Robinson, S. J., Cory, A. T., Florio, T., Concia, L., Juery, C., Schoonbeek, H., Steuernagel, B., Xiang, D., … Tan, Y. (2018). The transcriptional landscape of polyploid wheat. *Science*, *361*, eaar6089. https://doi.org/10.1126/science.aar6089

Raudvere, U., Kolberg, L., Kuzmin, I., Arak, T., Adler, P., Peterson, H., & Vilo, J. (2019). g:Profiler: A web server for functional enrichment analysis and conversions of gene lists (2019 update). *Nucleic Acids Research*, *47*, W191–W198. https://doi.org/10.1093/nar/gkz369

Rebetzke, G. J., Jimenez-Berni, J., Fischer, R. A., Deery, D. M., & Smith, D. J. (2019). Review: High-throughput phenotyping to enhance the use of crop genetic resources. *Plant Science*, *282*, 40–48. https://doi.org/10.1016/j.plantsci.2018.06.017

Ren, Y., He, X., Liu, D., Li, J., Zhao, X., Li, B., Tong, Y., Zhang, A., & Li, Z. (2012). Major quantitative trait loci for seminal root morphology of wheat seedlings. *Molecular Breeding*, *30*, 139–148. https://doi.org/10.1007/s11032-011-9605-7

Rexroad, C. E., & Vallejo, R. L. (2009). Estimates of linkage disequilibrium and effective population size in rainbow trout. *BMC Genetics*, *10*, Article 83. https://doi.org/10.1186/1471-2156-10-83

Reynolds, M., Atkin, O. K., Bennett, M., Cooper, M., Dodd, I. C., Foulkes, M. J., Frohberg, C., Hammer, G., Henderson, I. R., Huang, B., Korzun, V., Mccouch, S. R., Messina, C. D., Pogson, B. J., Slafer, G. A., Taylor, N. L., & Wittich, P. E. (2021). Addressing research bottlenecks to crop productivity. *Trends in Plant Science*, *26*, 607–630. https://doi.org/10.1016/j.tplants.2021.03.011

Reynolds, M., Foulkes, M. J., Slafer, G. A., Berry, P., Parry, M. A. J., Snape, J. W., & Angus, W. J. (2009). Raising yield potential in wheat. *Journal of Experimental Botany*, *60*(7), 1899–1918. https://doi.org/10.1093/jxb/erp016

Rich, S. M., Wasson, A. P., Richards, R. A., Katore, T., Prashar, R., Chowdhary, R., Saxena, D. C., Mamrutha, H. M., Zwart, A., Misra, S. C., Sai Prasad, S. V., Chatrath, R., Christopher, J., & Watt, M. (2016). Wheats developed for high yield on stored soil moisture have deep vigorous root systems. *Functional Plant Biology*, *43*, 173–188. https://doi.org/10.1071/FP15182

Richard, C. A., Hickey, L. T., Fletcher, S., Jennings, R., Chenu, K., & Christopher, J. T. (2015). High-throughput phenotyping of seminal root traits in wheat. *Plant Methods*, *11*, Article 13. https://doi.org/10.1186/s13007-015-0055-9

Salvi, S., & Tuberosa, R. (2015). The crop QTLome comes of age. *Current Opinion in Biotechnology*, *32*, 179–185. https://doi.org/10.1016/j.copbio.2015.01.001

Sanguineti, M. C., Li, S., Maccaferri, M., Corneti, S., Rotondo, F., Chiari, T., & Tuberosa, R. (2007). Genetic dissection of seminal root architecture in elite durum wheat germplasm. *Annals of Applied Biology*, *151*, 291–305. https://doi.org/10.1111/j.1744-7348.2007.00198.x

Segura, V., Vilhjálmsson, B. J., Platt, A., Korte, A., Seren, Ü., Long, Q., & Nordborg, M. (2012). An efficient multi-locus mixed-model approach for genome-wide association studies in structured populations. *Nature Genetics*, *44*, 825–830. https://doi.org/10.1038/ng.2314

Singh, D., Wang, X., Kumar, U., Gao, L., Noor, M., Imtiaz, M., Singh, R. P., & Poland, J. (2019). High-throughput phenotyping enabled genetic dissection of crop lodging in wheat. *Frontiers in Plant Science*, *10*, 394. https://doi.org/10.3389/fpls.2019.00394

Solovieff, N., Cotsapas, C., Lee, P. H., Purcell, S. M., & Smoller, J. W. (2013). Pleiotropy in complex traits: Challenges and strategies. *Nature Reviews Genetics*, *14*, 483–495. https://doi.org.org/10.1038/nrg3461

Soriano, J. M., & Alvaro, F. (2019). Discovering consensus genomic regions in wheat for root-related traits by QTL meta-analysis. *Scientific Reports*, *9*, Article 10537. https://doi.org/10.1038/s41598-019-47038-2

de Souza Campos, P. M., Cornejo, P., Rial, C., Borie, F., Varela, R. M., Seguel, A., & López-Ráez, J. A. (2019). Phosphate acquisition efficiency in wheat is related to root:Shoot ratio, strigolactone levels, and PHO2 regulation. *Journal of Experimental Botany*, *70*, 5631–5642. https://doi.org/10.1093/jxb/erz349

Steffens, B., & Rasmussen, A. (2016). The physiology of adventitious roots. *Plant Physiology*, *170*, 603–617. https://doi.org/10.1104/pp.15.01360

Sun, C., Hu, H., Cheng, Y., Yang, X., Qiao, Q., Wang, C., Zhang, L., Chen, D., Zhao, S., Dong, Z., & Chen, F. (2023). Genomics-assisted breeding: The next-generation wheat breeding era. *Plant Breeding*, *142*, 259–268. https://doi.org.org/10.1111/pbr.13094

Sved, J. A. (1971). Linkage disequilibrium and homozygosity of chromosome segments in finite populations. *Theoretical Population Biology*, *2*, 125–141. https://doi.org/10.1016/0040-5809(71)90011-6

Tardieu, F., Cabrera-Bosquet, L., Pridmore, T., & Bennett, M. (2017). Plant phenomics, from sensors to knowledge. *Current Biology*, *27*, R770–R783. https://doi.org/10.1016/j.cub.2017.05.055

The R Core Team. (2016). *R: A language and environment for statistical computing*. CRAN.

Tidiane Sall, A., Chiari, T., Legesse, W., Seid-Ahmed, K., Ortiz, R., Van Ginkel, M., & Bassi, F. M. (2019). Durum wheat (*Triticum durum* Desf.): Origin, cultivation and potential expansion in sub-Saharan Africa. *Agronomy*, *9*, 263. https://doi.org/10.3390/agronomy9050263

Trejo, C., Else, M. A., & Atkinson, C. J. (2018). Responses of seminal wheat seedling roots to soil water deficits. *Journal of Plant Physiology*, *223*, 105–114. https://doi.org/10.1016/j.jplph.2018.03.002

Tuberosa, R. (2012). Phenotyping for drought tolerance of crops in the genomics era. *Frontiers in Physiology*, *3*, Article 347. https://doi.org.org/10.3389/fphys.2012.00347

Tuberosa, R., Frascaroli, E., Maccaferri, M., & Salvi, S. (2021). Understanding and exploiting the genetics of plant root traits. In *Understanding and improving crop root function* (pp. 395–466). Burleigh Dodds Science Publishing. https://doi.org/10.19103/AS.2020.0075.21

Tuberosa, R., & Salvi, S. (2006). Genomics-based approaches to improve drought tolerance of crops. *Trends Plant Science*, *11*, 405–412. https://doi.org/10.1016/j.tplants.2006.06.003

Uga, Y., Sugimoto, K., Ogawa, S., Rane, J., Ishitani, M., Hara, N., Kitomi, Y., Inukai, Y., Ono, K., Kanno, N., Inoue, H., Takehisa, H., Motoyama, R., Nagamura, Y., Wu, J., Matsumoto, T., Takai, T., Okuno, K., & Yano, M. (2013). Control of root system architecture by DEEPER ROOTING 1 increases rice yield under drought conditions. *Nature Genetics*, *45*(9), 1097–1102. https://doi.org/10.1038/ng.2725

Vadez, V., Grondin, A., Chenu, K., Henry, A., Laplaze, L., Millet, E. J., & Carminati, A. (2024). Crop traits and production under drought. *Nature Reviews Earth and Environment*, *5*, 211–225. https://doi.org.org/10.1038/s43017-023-00514-w

Varshney, R. K., Sinha, P., Singh, V. K., Kumar, A., Zhang, Q., & Bennetzen, J. L. (2020). 5Gs for crop genetic improvement. *Current Opinion in Plant Biology*, *56*, 190–196. https://doi.org/10.1016/j.pbi.2019.12.004

Wang, S., Wong, D., Forrest, K., Allen, A., Chao, S., Huang, B. E., Maccaferri, M., Salvi, S., Milner, S. G., Cattivelli, L., Mastrangelo, A. M., Whan, A., Stephen, S., Barker, G., Wieseke, R., Plieske, J., Lillemo, M., Mather, D., … Akhunov, E. (2014). Characterization of polyploid wheat genomic diversity using a high-density 90 000 single nucleotide polymorphism array. *Plant Biotechnology Journal*, *12*(6), 787–796. https://doi.org/10.1111/pbi.12183

Wasson, A. P., Richards, R. A., Chatrath, R., Misra, S. C., Prasad, S. V. S., Rebetzke, G. J., Kirkegaard, J. A., Christopher, J., & Watt, M. (2012). Traits and selection strategies to improve root systems and water uptake in water-limited wheat crops. *Journal of Experimental Botany*, *63*, 3485–3498. https://doi.org/10.1093/jxb/ers111

Weihs, B. J., Heuschele, D. J., Tang, Z., York, L. M., Zhang, Z., & Xu, Z. (2024). The state of the art in root system architecture image analysis using artificial intelligence: A review. *Plant Phenomics*, *6*, 0178. https://doi.org.org/10.1002/fes3.70024

Wickham, H., Chang, W., Henry, L., Pedersen, T. L., Takahashi, K., Wilke, C., Woo, K., Yutani, H., Dunnington, D., & van den Brand, T., & Posit, PBC. (2025). ggplot2: Create Elegant Data Visualisations Using the Grammar of Graphics (Version 4.0.0) [Computer software]. CRAN.

Wickham, H., François, R., Henry, L., & Muller, K. (2022). *Dplyr: A grammar of data manipulation* [R package version 1.0.10]. https://CRAN.R-project.org/package=dplyr

York, L. M., Slack, S., Bennett, M. J., & Foulkes, M. J. (2018). Wheat shovelomics I: A field phenotyping approach for characterising the structure and function of root systems in tillering species. *BioRxiv*, 280875. https://doi.org/10.1101/280875

Yu, P., Gutjahr, C., Li, C., & Hochholdinger, F. (2016). Genetic control of lateral root formation in cereals. *Trends in Plant Science*, *21*, 951–961. https://doi.org/10.1016/j.tplants.2016.07.011

Zeng, Z., Wu, W., Li, Y., Huang, C., Zhang, X., Peñuelas, J., Zhang, Y., Gentine, P., Li, Z., Wang, X., Huang, H., Ren, X., & Ge, Q. (2023). Increasing meteorological drought under climate change reduces terrestrial ecosystem productivity and carbon storage. *One Earth*, *6*, 1326–1339. https://doi.org/10.1016/j.oneear.2023.09.007

Zhang, X. X., Whalley, P. A., Ashton, R. W., Evans, J., Hawkesford, M. J., Griffiths, S., Huang, Z. D., Zhou, H., Mooney, S. J., & Whalley, W. R. (2020). A comparison between water uptake and root length density in winter wheat: Effects of root density and rhizosphere properties. *Plant and Soil*, *451*(1–2), 345–356. https://doi.org/10.1007/s11104-020-04530-3

Zhou, Y., Browning, S. R., & Browning, B. L. (2020). A fast and simple method for detecting identity-by-descent segments in large-scale data. *The American Journal of Human Genetics*, *106*, 426–437. https://doi.org/10.1016/j.ajhg.2020.02.010

SUPPORTING INFORMATION

Additional supporting information can be found online in the Supporting Information section at the end of this article.

How to cite this article: Sciara, G., Bozzoli, M., Fiorani, F., Nagel, K. A., Ameer, A., Salvi, S., Tuberosa, R., & Maccaferri, M. (2025). Genetic dissection of the root system architecture QTLome and its relationship with early shoot development, breeding and adaptation in durum wheat. *The Plant Genome*, *18*, e70146. https://doi.org/10.1002/tpg2.70146